Cell Metabolism

Article

# An isocaloric moderately high-fat diet extends lifespan in male rats and *Drosophila*

## Graphical abstract

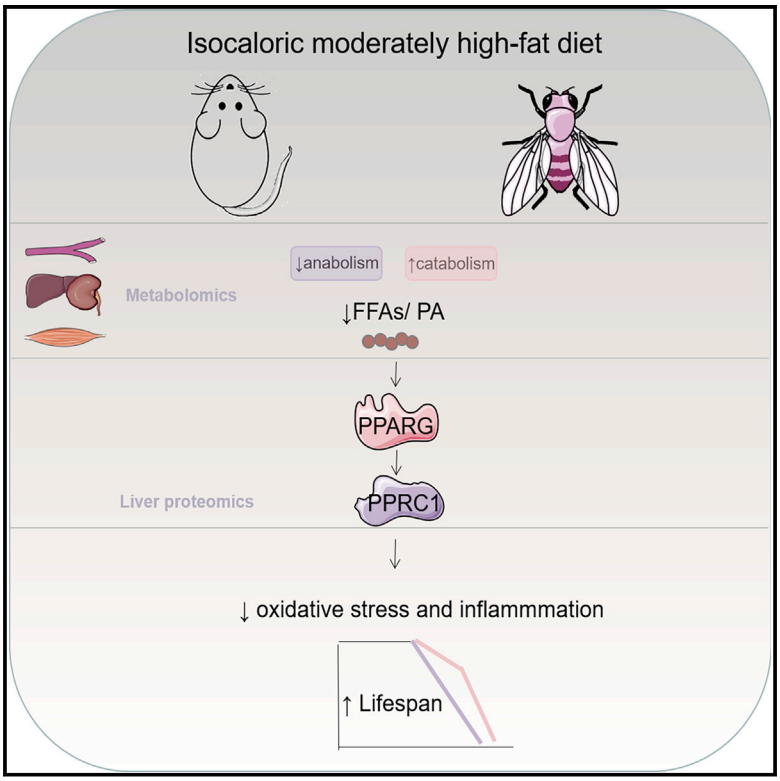


## Highlights

- An IHF extends lifespan in male rats and flies
- The IHF decreases the profiles of FFAs in serum and multiple tissues in rats and flies
- The IHF downregulates anabolism of FFAs and upregulates catabolism of FFAs
- Decreased FFAs upregulate PPRC1, mediating the effect of IHF on lifespan via PPARG

## Authors

Dan Shi, TianShu Han, Xia Chu, ..., YuCun Niu, Ying Li, ChangHao Sun

## Correspondence

niuyucun@163.com (Y.N.), liying_helen@163.com (Y.L.), changhaosun2002@163.com (C.S.)

## In Brief

Shi et al. demonstrated that an isocaloric moderately high-fat diet extended lifespan in male rats and *Drosophila* by decreasing free fatty acids in serum and multiple tissues. They also identified and validated a new aging pathway that was regulated by free fatty acids in rats, *Drosophila*, and human.

Shi et al., 2021, Cell Metabolism *33*, 581–597
March 2, 2021 
https://doi.org/10.1016/j.cmet.2020.12.017

CellPress

Cell Metabolism

CellPress

Article

# An isocaloric moderately high-fat diet extends lifespan in male rats and *Drosophila*

Dan Shi,[1,3] TianShu Han,[1,3] Xia Chu,[1] Huimin Lu,[1] Xue Yang,[1] TianQi Zi,[1] YanHe Zhao,[1] XinYue Wang,[1] ZhiPeng Liu,[1] JingQi Ruan,[1] Xin Liu,[1] Hua Ning,[1] MaoQing Wang,[1] Zhen Tian,[1] Wei Wei,[1] Yue Sun,[1] YinLing Li,[1] Rui Guo,[1] Yu Wang,[1] Fan Ling,[1] Yue Guan,[1] Da Shen,[2] YuCun Niu,[1,*] Ying Li,[1,*] and ChangHao Sun[1,4,*]

[1]National Key Discipline Laboratory, Department of Nutrition and Food Hygiene, School of Public Health, Harbin Medical University, Harbin, P.R. China

[2]Gene Regulatory Laboratory, School of Medicine, Tsinghua University, Beijing 100084, China

[3]These authors contributed equally

[4]Lead contact

*Correspondence: niuyucun@163.com (Y.N.), liying_helen@163.com (Y.L.), changhaosun2002@163.com (C.S.)

https://doi.org/10.1016/j.cmet.2020.12.017

## Summary

The health effect of dietary fat has been one of the most vexing issues in the field of nutrition. Few animal studies have examined the impact of high-fat diets on lifespan by controlling energy intake. In this study, we found that compared to a normal diet, an isocaloric moderately high-fat diet (IHF) significantly prolonged lifespan by decreasing the profiles of free fatty acids (FFAs) in serum and multiple tissues via downregulating FFA anabolism and upregulating catabolism pathways in rats and flies. Proteomics analysis in rats identified PPRC1 as a key protein that was significantly upregulated by nearly 2-fold by IHF, and among the FFAs, only palmitic acid (PA) was robustly and negatively associated with the expression of PPRC1. Using PPRC1 transgenic RNAi/overexpression flies and *in vitro* experiments, we demonstrated that IHF significantly reduced PA, which could upregulate PPRC1 through PPARG, resulting in improvements in oxidative stress and inflammation and prolonging the lifespan.

## Introduction

The health effects of dietary fat have been among the most vexing issues in public health. Although dietary recommendations have universally advocated that energy provided by dietary fat should not exceed 30% for maintaining health, the recent US dietary guideline has canceled the upper limit of fat intake based on evidence showing that replacing total fat with other macronutrients does not lower the risk of cardiometabolic diseases (Mozaffarian and Ludwig, 2015; Siri-Tarino et al., 2010). Most recently, in 2017, pioneering research further pointed out that a high-fat diet decreases the risk of mortality and vascular disease (Dehghan et al., 2017). Indeed, the health effects exerted by dietary fat could be modified by additional factors, such as calories, as the higher energy provision of fat is accompanied by higher energy intake, delineating the complexity of the mixed effect of dietary composition on health (DeClerck, 2016; Piper and Bartke, 2008; Wu et al., 2019). Therefore, to elucidate the health effects of dietary fat, it is necessary to design a rigorous long-term experiment controlling the total energy intake. However, such experiments are difficult and infeasible to perform in humans.

In these circumstances, animal studies controlling energy intake and feeding high fat throughout adulthood may provide important evidence for the health effects of dietary fat. Currently, few studies have investigated the health effects of dietary fat while controlling the total energy intake; among these, two studies are worth emphasizing. One study adopted an intervention of an isocaloric diet with 60% of the energy from fat (Lundsgaard et al., 2019), and the other study adopted an intervention of an isocaloric diet with 90% of the energy from fat (Roberts et al., 2018), both compared to a control diet. Although both the studies have demonstrated the potential beneficial effects of dietary fat, the durations of the experiments were relatively short, or the intervention doses were extremely high. The long-term health effects of more moderate high-fat percentages under the condition of controlling the total energy intake remain largely unknown. In this study, we performed a series of long-term rat and *Drosophila* experiments with rigorous feeding of an isocaloric moderately high-fat (IHF) diet (35% energy from fat) throughout the life cycle. The energy intake was based on the control group, which was fed a normal diet ad libitum during the experiment. We aimed to elucidate whether and how an IHF diet would impact lifespan.

Our data showed that an IHF diet significantly prolonged lifespan and delayed age-associated physiological declines in both rats and flies. Unexpectedly, an IHF diet significantly decreased free fatty acids (FFAs) in both serum and peripheral tissues, including liver, kidney, and muscle, by downregulating

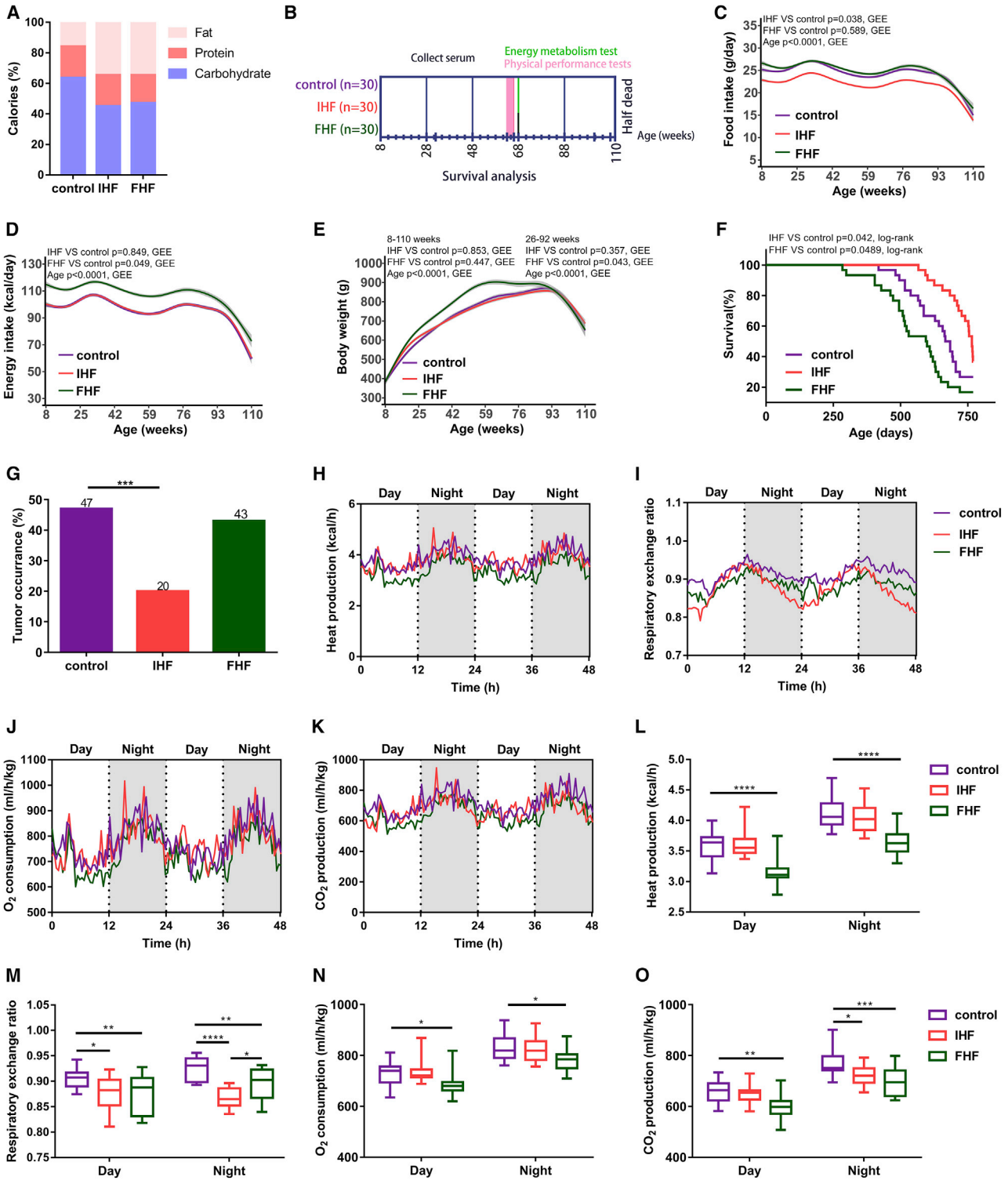


**Figure 1. IHF prolongs lifespan and delays tumor occurrence and effects on energy metabolic profiles in rats**

(A) Diet composition in male rats.

(B) Schematic illustration of the experimental design in male rats.

(C) Food intake trajectories (n = 30 rats per group in the beginning).

(D) Energy intake trajectories (n = 30 rats per group in the beginning).

(E) Bodyweight trajectories (n = 30 rats per group in the beginning).

(legend continued on next page)

FFA anabolism and upregulating catabolism pathways, and these observations were consistently repeated in the flies. Using a proteomics approach, PPRC1 was identified as a key protein that was significantly upregulated by the IHF diet by nearly 2-fold. Among the decreased profiles of FFAs, only palmitic acid (PA) was robustly and negatively associated with the expression of PPRC1. Using PPRC1 transgenic RNAi/overexpression flies and a series of *in vitro* experiments, we first demonstrated that the IHF diet significantly reduced PA, which could upregulate PPRC1 through PPARG, prolong lifespan, and improve oxidative stress and inflammation.

## Results

### IHF prolongs the lifespan and healthspan of rats

Ninety Wistar rats were randomly divided into three groups and fed three diets for 2 years: normal diet ad libitum (control), IHF, and free-eating high-fat diet (FHF) (Figures 1A, 1B, and S1A). Food intake was rigorously monitored and adjusted dynamically to achieve constant energy intake between the control and IHF groups, while energy intake in the FHF group was significantly higher (Figures 1C and 1D). The body weight, multiple organ weights, and muscle weights did not differ between the control and IHF groups (Figures 1E, S1B, and S1C), whereas the visceral fat content of rats was significantly lower in the IHF group than in the control group (Figure S1D).

Compared to the control diet, IHF significantly prolonged the median lifespan by 90 days, whereas FHF significantly decreased the median lifespan by 79 days (Figure 1F). A detailed necropsy and gross pathological examination of dead rats suggested that rats exposed to IHF had a reduction in the type and number of some pathologies, including aspects of fibrosis, transparent degeneration, and hyperplasia (Table S1). Overall, tumor occurrence was lower in the IHF diet than the control diet, while a FHF diet did not induce tumor formation (Figures 1G and S1E), which was confirmed by pathology examination (Table S2). Moreover, the age-associated pathological injuries in the lung, kidney, and liver measured by organ pathological analysis prepared from aged rats were also remarkably mitigated in the IHF group, which were revealed by a decreasing trend in broncheoli-associated lymphoid tissue in the lung (Figure S2A), a reduction in tubular luminal space and urinary casts in the kidney (Figures S2B and S2C), and hepatic activity index (HAI) in the liver (Figure S2D), reflected by a significant decrease in periportal/bridging necrosis (Figure S2E), portal inflammation (Figure S2F), and fibrosis (Figure S2G) with a decreasing trend in intralobular degeneration and focal necrosis (Figure S2H). In contrast, age-associated pathological injuries of broncheoli-associated lymphoid tissue in the lung and tubular luminal space in the kidney were significantly increased in the FHF group relative to the control group (Figures S2A and S2B).

As energy metabolism could be a driver of aging (Feng et al., 2016), we further attempted to measure the influences of diets on energy expenditure in rats aged 68 weeks. During the test, the average caloric intake did not differ between the IHF group and the control group, although the average food consumption was lower (Figure S1F), the average caloric intake was higher in the FHF group (Figure S1F). Indirect calorimetry revealed no significant differences in heat production in the IHF group compared to the control (Figures 1H and 1L), but heat production was lower in the FHF group (Figures 1H and 1L). The respiratory exchange ratio was obviously reduced in the IHF group and the FHF group (Figures 1I and 1M), but the reduction in the IHF group was larger than that in the FHF group during the dark phases ($p < 0.01$), suggesting a preference for fat utilization. Compared to control, oxygen consumption showed no statistical change upon IHF but was decreased upon FHF (Figures 1J and 1N). Moreover, carbon dioxide production was significantly reduced by either an IHF diet or a FHF diet compared to the control paradigm (Figures 1K and 1O). All the results were adjusted for body weight.

We next determined whether an IHF could have broader effects on healthspan; thus, memory and physical performance tests were implemented in rats aged 63–66 weeks. The error response times were slightly reduced, and the percentage of conditional responses in the shuttle box test was significantly higher in the IHF group than in the control group (Figure S1G), indicating the benefits of an IHF on cognition. No significant differences were shown in the Morris water maze (MWM) test, including escape latency (Figure S1H), percentage of time in the training quadrant (Figure S1I), percentage of path length in the target quadrant (Figure S1J), and platform crossings (Figure S1K). Running distances tended to be lengthened in the treadmill test in the IHF group compared with the control group (Figure S1L), suggesting an improvement trend in the general fitness of rats. In most cases, FHF group performance tended to be worse than the control. Combined, the results suggest that an IHF diet not only extends the lifespan of rats but also improves many aspects of health in the whole body.

### Trajectories of biomarkers of aging during the experiment

Biomarkers that can evaluate biological aging were dynamically measured during the experiment (Bonadonna et al., 1994; Longo et al., 2015; López-Otín et al., 2013). Aging in rats was characterized by a significant increase or decrease in all these biomarkers, including glucose (GLU), total cholesterol (TCHO), triglyceride (TG), low-density lipoprotein cholesterol (LDL-C), high-density lipoprotein cholesterol (HDL-C),

(F) Survival curves for IHF and FHF versus control in male rats. Lifespan was extended in response to the IHF diet ($p = 0.042$, log-rank) but shortened in response to the FHF diet ($p = 0.0489$, log-rank) ($n = 30$ rats per group).
(G) Tumor occurrence in animals (control, $n = 30$ rats; IHF, $n = 30$ rats; FHF, $n = 30$ rats).
(H–O) Energy metabolism in male rats during two 24 h cycles using indirect calorimetry ($n = 15$ rats per group, 68 weeks, male). For rats assigned to the IHF cohorts, food was supplied on the basis of the control to maintain identical energy intake.
(H–K) Temporal patterns of (H) heat production, (I) respiratory exchange ratio, (J) oxygen consumption, and (K) carbon dioxide production are shown.
(L–O) Bar chart of (L) heat production, (M) respiratory exchange ratio, (N) oxygen consumption, and (O) carbon dioxide production is shown.
Data in (H)–(K) are presented as mean. Error bars, when present, show the SEM. Statistical analyses were performed using the generalized estimating equation (GEE) for (C)–(E). *$p < 0.05$; **$p < 0.01$; ***$p < 0.001$; ****$p < 0.0001$. See also Figures S1 and S2 and Data S1.

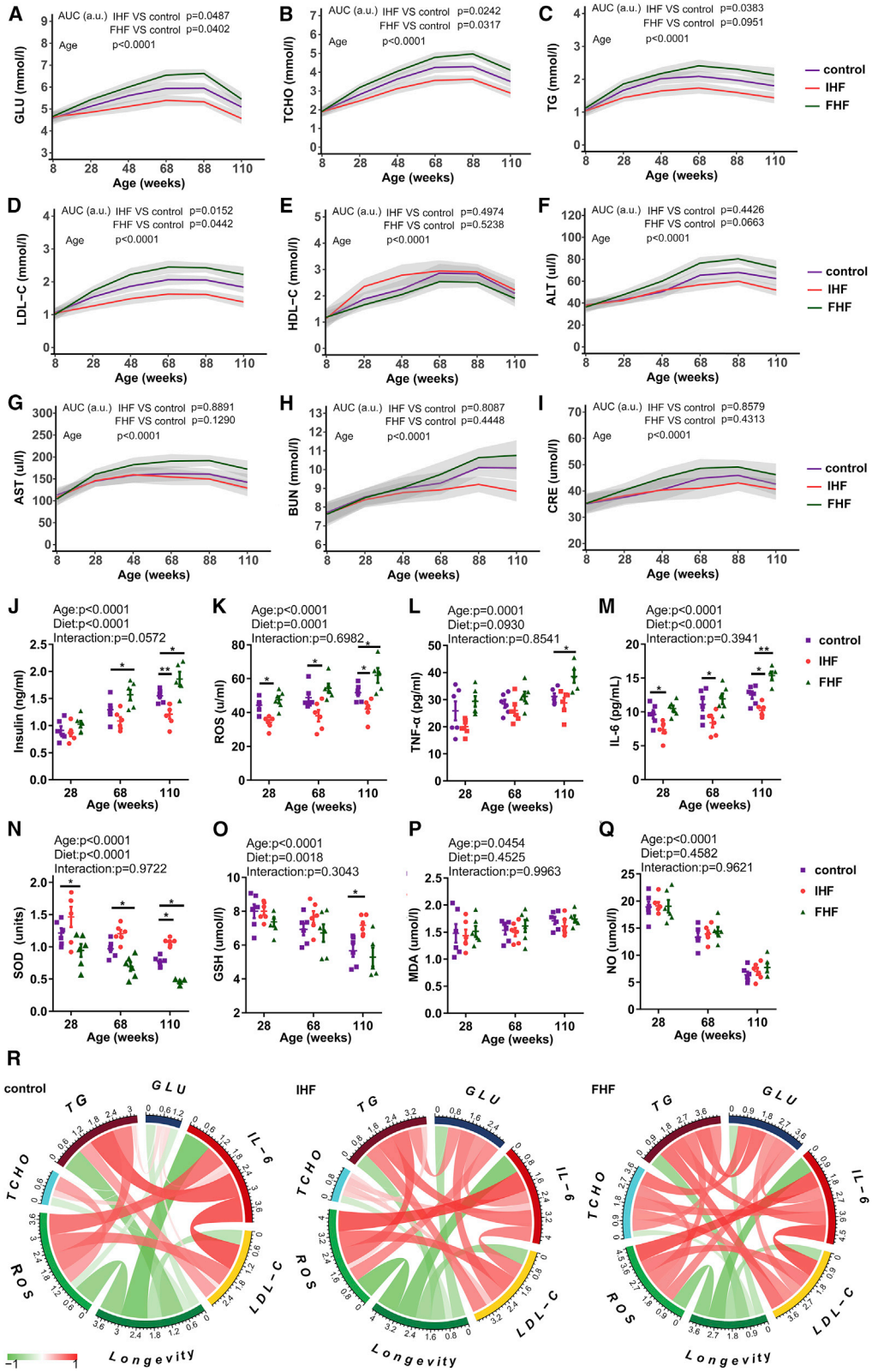


*(legend on next page)*

alanine aminotransferase (ALT), aspartate aminotransferase (AST), blood urea nitrogen (BUN), creatinine (CRE), insulin, reactive oxygen species (ROS), tumor necrosis factor-alpha (TNF-α), interleukin-6 (IL-6), superoxide dismutase (SOD), glutathione (GSH), malondialdehyde (MDA), and nitric oxide (NO), but several of these variables were observed to be significantly decreased with IHF intervention (Figures 2A–2Q), whereas FHF intervention led to a significant increase in the majority of these parameters (Figures 2A–2Q). Correlation analysis performed at 68 weeks further suggested that among these differential aging biomarkers, decreased ROS and IL-6 mediated the effects of IHF on lifespan extension (Figure 2R), suggesting that IHF could ameliorate inflammatory and oxidative stress.

### Profiles of fatty acids in serum, liver, kidney, and muscle

Given that the respiratory exchange ratio in the IHF group was obviously reduced compared to the other two diets in rats (Figures 1I and 1M), which suggests that the IHF may utilize fat as the main fuel source for energy expenditure and accelerate fat metabolism, we measured the profiles of FFAs in serum and multiple tissues, including liver, kidney, and muscle. Total FFAs were significantly lower in the IHF group than in the control group, whereas FHF had the highest FFA levels (Figures 3A–3D). Among these different types of FFAs, only PA (C16:0) in the IHF group was consistently decreased in serum, liver, kidney, and muscle (Figures 3A–3D). Further, several enzymes involved in fatty acid metabolism in the liver or muscle were measured. The IHF downregulated the hepatic and muscular protein levels of fatty acid synthase (FAS) and acetyl-CoA carboxylase (ACC) (Figures 3E–3G and 3J–3L), which are key proteins involved in the fatty acid synthesis. Moreover, it upregulated hepatic or muscular protein expression of carnitine palmitoyltransferase 1A (CPT1A) and carnitine palmitoyltransferase 2 (CPT2) (Figures 3E, 3H–3J, and 3M), which are essential enzymes involved in β-oxidation of long-chain fatty acids. Taken together, these results indicated that the IHF accelerated fat metabolism by decreasing total FFAs and PA in serum, liver, kidney, and muscle by downregulating the fatty acid synthesis and upregulating fatty acid metabolism. Because the effect of FFAs on inflammatory and oxidative stress has been abundantly reported (Inoguchi et al., 2000; Pereira et al., 2014; Tripathy et al., 2003), we hypothesize that an IHF would decrease the profiles of FFAs and some types of FFAs, which may result in improved oxidative stress, inflammation, and extended lifespan.

### Liver proteomic changes further reflected the above observations and identified PPRC1 as a candidate target

To elucidate how the IHF extended the lifespan of the rats, a global proteomic analysis was performed on liver samples of aging rats. The total number of differentially expressed proteins in the IHF group compared to the control group was 571 with 139 upregulated and 432 downregulated, while in the FHF group was 311 with 187 upregulated and 124 downregulated (Figure 4A). Since nutrient-sensing signaling pathways are widely involved in longevity regulation (Fontana et al., 2010), we first investigated the pathway change in response to the IHF in our proteomic data. Significantly altered proteins in the IHF group enriched in ribosome item and classic nutrient-sensing signaling pathways involved in longevity regulation were mostly downregulated, including mTOR signaling pathway, PI3K-Akt signaling pathway, and insulin signaling pathway (Figure S3A). However, in most instances, this similar change was not observed upon FHF (Figure S3B). In addition, we found that Kyoto encyclopedia of genes and genomes (KEGG) and gene ontology (GO) enrichment analyses of significantly altered proteins in the IHF group identified remarkably significantly downregulated pathways implicated in protein processing and transportation, such as Golgi vesicle transport (Figures S3C and S3D). These above findings are consistent with the notion that benefits in aging studies in multiple species probably come from the assumption of "less is better"—less food, less growth/insulin-like growth factor-1 signaling, less protein translation, etc. (Hofmann et al., 2015; López-Otín et al., 2013), as further illustrated by the differential downregulation of all the network center proteins (Figure S3E).

To further examine why the IHF extended lifespan, we observed that the IHF could improve oxidative stress and fatty acid metabolism. As expected, enrichment analysis of differential proteins in the IHF group also related downregulated pathways and items to the IL-17 signaling pathway, inflammatory response, response to ROS, regulation of I-kappaB kinase/NF-kappaB cascade, and response to oxidative stress (Figure 4B), indicative of the inhibition of oxidative stress and inflammation response. In contrast to the IHF, proteins in oxidative stress and inflammation were mostly upregulated upon FHF (Figure 4C). Differential proteins upon IHF related to oxidative stress and inflammation were plotted using STRING and cytoscape (Figure 4D). The hub proteins of the cluster of differentiation 36 (CD36) and catalase (CAT) in the network were selected for further validation (Figure 4D). In accordance with the proteomic results, we observed persistent upregulation of CAT in liver and muscle tissues (Figures 4E, 4F, 4J, and 4K),

**Figure 2. IHF effects on blood biochemistry variables of glucose, lipids, liver/kidney function, oxidative stress, and inflammation**

(A–I) Serum chemistry measures of glucose, lipid levels, and liver/kidney function in male rats. Serum concentrations of (A) glucose (GLU), (B) TCHO, (C) triglycerides (TG), (D) low-density lipoprotein cholesterol (LDL-C), (E) high-density lipoprotein cholesterol (HDL-C), (F) alanine aminotransferase (ALT), (G) aspartate aminotransferase (AST), (H) BUN, and (I) creatinine (CRE) at weeks 8, 28, 48, 68, 88, and 110 (control, n = 6–8 rats; IHF, n = 6–8 rats; FHF, n = 5–8 rats).

(J–Q) Serum parameters of oxidative stress and inflammation. Serum concentrations of (J) insulin, (K) ROS, (L) tumor necrosis factor alpha (TNF-α), (M) interleukin 6 (IL-6), (N) superoxide dismutase (SOD), (O) glutathione (GSH), (P) malondialdehyde (MDA), and (Q) nitric oxide (NO) at weeks 28, 68, and 110 (control, n = 6–8 rats; IHF, n = 6–8 rats; FHF, n = 5–8 rats).

(R) Pearson correlations among significant serum measures and survival days were conducted in rats aged 68 weeks (left, control group; middle, IHF group; right, FHF group). The correlation between each pair of parameters is shown. IL-6 and ROS were robustly and negatively correlated with longevity (the correlation coefficients for IL-6 were −0.99, −0.939, and −0.936, respectively, in the three groups, $p < 0.001$; the correlation coefficients for ROS were −0.82, −0.968, and −0.849, respectively, in the three groups, $p < 0.05$). The color and width of the line represent the correlation coefficient. Red lines represent positive correlations, and green lines represent negative correlations (control, n = 6–8 rats; IHF, n = 6–8 rats; FHF, n = 6–8 rats).

Error bars, when present, show the SEM. Pearson correlation analysis test for (R). *$p < 0.05$; **$p < 0.01$; ***$p < 0.001$; ****$p < 0.0001$.

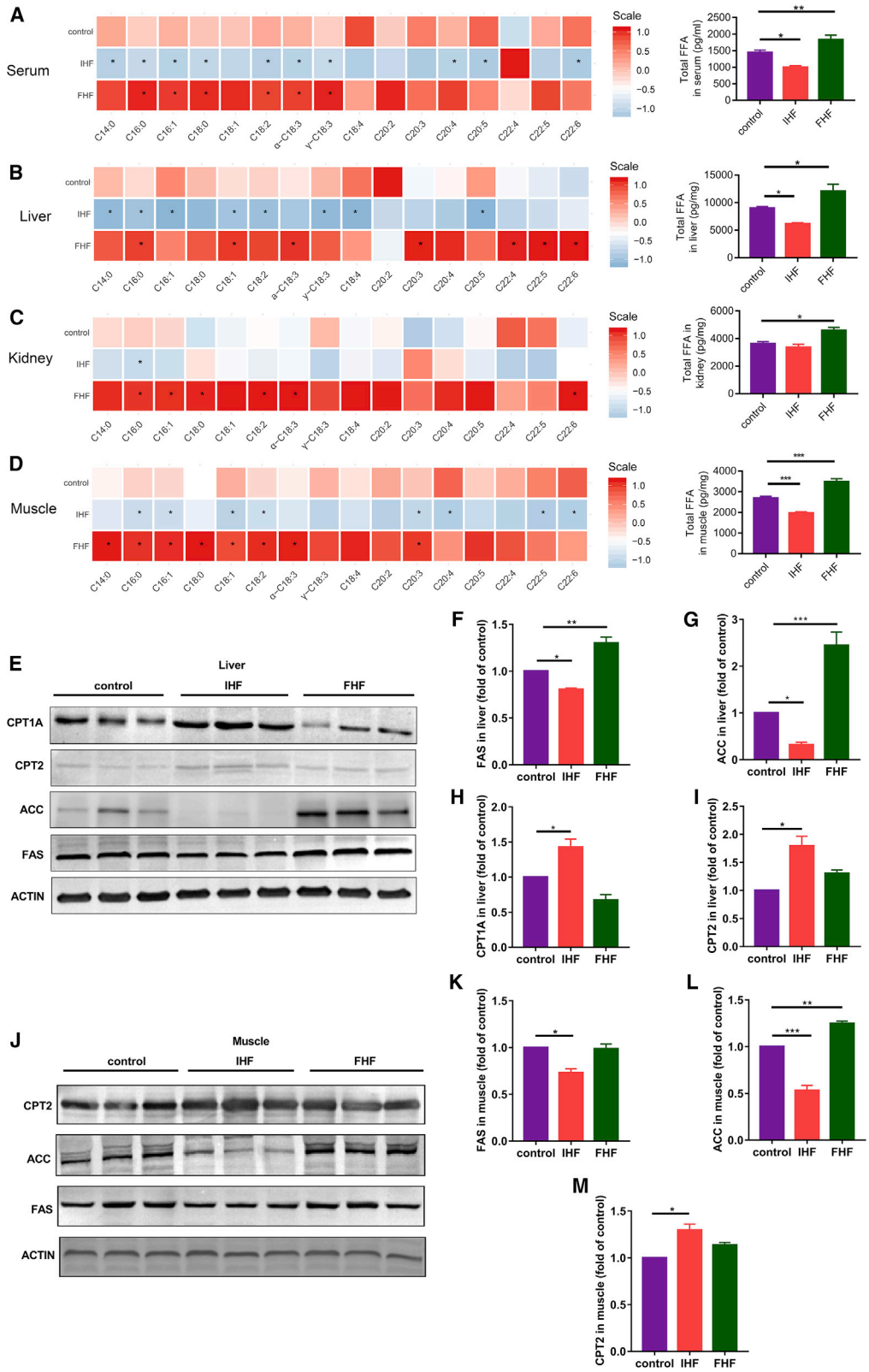


**Figure 3. IHF effects on free fatty acid profiles in serum, liver, kidney, and muscle**

(A–E) IHF lowered FFA profiles (left) and total FFA concentration (right) in (A) serum, (B) liver, (C) kidney, (D) muscle at 68 weeks (control, n = 8 rats; IHF, n = 8 rats; FHF, n = 8 rats). *Compared with control, $p < 0.05$.

*(legend continued on next page)*

which probably enhances survival by protecting the cell from oxidative damage by ROS (Schriner and Linford, 2006), and downregulation of CD36 in liver and muscle tissues (Figures 4E, 4G, 4J, and 4L), which is involved in the proinflammatory process by targeting NLRP3 inflammasome activation (Abumrad and Goldberg, 2016; Sheedy et al., 2013), thus representing a consistent effect of IHF on counteracting oxidative stress and inflammation. Consistently, we further examined the downregulated hepatic and muscular levels of nuclear factor kappa-B p65 (NF-κB P65, P65) and IL-6 involved in the classic inflammatory pathway, indicating that suppression of the effect may occur in multiple ways (Figures 4E, 4H–4J, 4M, and 4N). Moreover, consistent with the decreased profiles of FFAs in the IHF group documented above, the protein levels of several enzymes linked to fatty acid biosynthetic processes in the liver, including prostaglandin G/H synthase 1 (PTGS1), Leukotriene A(4) hydrolase (LTA4H), and cytochrome c oxidase subunit 2 (MT-$CO_2$), were also downregulated (Figure 4B).

More importantly, to identify a key protein involved in IHF-mediated lifespan extension, proteins of synthase kinase-3β (GSK-3β), flotillin-1 (FLOTTIN), neurocalcin delta (NCALD), and peroxisome proliferative-activated receptor-gamma coactivator-related 1 (PPRC1) were identified based on the fold change or centered in the protein-protein interaction (PPI) network (Figure 5A), which were further confirmed by western blot experiments in liver and muscle tissues (Figures 5B–5K). Based on the above hypothesis, the relationship between the profiles of FFAs and the mRNA expressions of the four proteins was examined. Among these proteins, only PPRC1 was robustly and negatively related to PA (Figure 5L), and its protein level was upregulated, on average, 2-fold with the IHF in both liver and muscle tissues of rats compared with the control diet (Figures 5A, 5B, 5F, 5G, and 5K). Indeed, a study reported that overexpression of the *Drosophila* homolog of PPRC1 leads to an increase in lifespan (Rera et al., 2011), indicating a vital role in aging. We further confirmed that PPRC1 expression decreased with age in the liver and kidney tissue of rats (Figures 5M–5P). Therefore, the relationship between PA and PPRC1 seemed to play an important role in regulating the effect of IHF on prolonged lifespan.

## IHF also prolonged the lifespan in flies

To examine whether the effect of an IHF on prolonged lifespan could be repeated in flies, a series of experiments using flies were performed. We first designed IHF and FHF paradigms for *Drosophila* (Table S3) and performed survival assays with three different concentrations of lard in the diet in the $w^{1118}$ strains (Figure 6A). An effect of the IHF containing 7% (w/v) lard on the prolonged lifespan was observed in $w^{1118}$, and the same was true for attp2 flies (Figures 6B and 6C). Food intake was not different in $w^{1118}$ or attp2 between the IHF and control groups, indicating that energy intake was equal between the diets (Figures 6D and 6E). Analogous to the results in the rat study, total FFAs and PA were also significantly decreased in the IHF group (Figures 6F and 6G), and the mRNA expression of *Drosophila* homologous PPRC1 (dh-PPRC1) was also upregulated (Figure 6H). We also detected persistent mRNA expression with respect to oxidative stress, inflammation, and fatty acid metabolism, as illustrated by upregulation of cat (homolog of catalase), whd (homolog of cpt1), and cpt2, as well as downregulation of dorsal (homolog of p65) in the IHF group, despite no change in crq (homolog of cd36) or acc (Figures 6H and 6I).

To elucidate whether and how the relationship between PA and PPRC1 is involved in the effect of the IHF on lifespan, flies were first fed PA in the diet. Flies from either the $w^{1118}$ or attp2 strains reared on PA showed significantly decreased lifespan with control diet, while the reduction was larger with the IHF, suggesting that decreased PA may contribute to IHF-mediated lifespan extension (Figures 6B and 6C). Flies treated with IHF+PA showed a higher level of some FFAs, higher expression of oxidative stress and inflammation genes, and lower mRNA expression of *Drosophila* homologous PPRC1 (dh-PPRC1) than those treated with the IHF alone (Figures 6F–6H). These results indicated that PA caused increased levels of oxidative stress and inflammation and regulated the expression of *Drosophila* homologous PPRC1 in response to the IHF.

## Transgenic RNAi and overexpression flies

Further, we examined whether dh-PPRC1 and PA were involved in the effect of IHF on prolonged lifespan in male flies lacking the *Drosophila* homologous PPRC1. As knockout PPRC1 mice show embryonic lethality, we attempted to use the constitutive daGAL4, ubiGAL4, or tubGAL4 driver line to inhibit dh-PPRC1 expression. IHF extended lifespan in wild-type flies and dh-PPRC1 RNAi mutants driven by daGAL4, ubiGAL4, or tubGAL4, but lifespan extension upon IHF in wild-type flies was persistently larger than that in dh-PPRC1 RNAi mutants, demonstrating that PPRC1 primarily contributes to IHF-mediated lifespan extension (Figures 6J, 6K, and S4). In addition, PA impaired IHF-mediated lifespan extension in both wild-type flies and dh-PPRC1 RNAi1 mutants driven by daGAL4, ubiGAL4 or tubGAL4 lines, but lifespan impairment driven by PA upon IHF in wild-type flies was also persistently larger than that in dh-PPRC1 RNAi1 mutants (Figures 6J, 6K, and S4), further suggesting that dh-PPRC1 was involved in the effect of decreased PA on IHF in terms of lifespan extension. To further demonstrate the importance of dh-PPRC1 and PA for the effects of the IHF on lifespan extension, we overexpressed the dh-PPRC1 gene driver by daGAL4 in all other tissues to measure the effect of the IHF on lifespan in flies reared on PA. We observed that dh-PPRC1 overexpression flies reared on PA partially rescued the impaired lifespan upon IHF (Figure 6L). We also found that dh-PPRC1 overexpression flies treated with PA showed partial restoration of impaired oxidative

(E–I) Protein levels of fatty acid metabolism in the liver were measured by western blot at 110 weeks.
(E) Representative blots are shown for each protein. A representative loading control is shown for each case (n = 3).
(F–I) Quantification of (F) FAS, (G) ACC, (H) CPT1A, and (I) CPT2 protein levels.
(J–M) Protein levels of fatty acid metabolism in the muscle were measured by western blot at 110 weeks.
(J) Representative blots are shown for each protein. A representative loading control is shown for each case (n = 3).
(K–M) Quantification of (K) FAS, (L) CPT2, and (M) ACC protein levels.
Error bars, when present, show the SEM. *$p < 0.05$; **$p < 0.01$; ***$p < 0.001$; ****$p < 0.0001$.

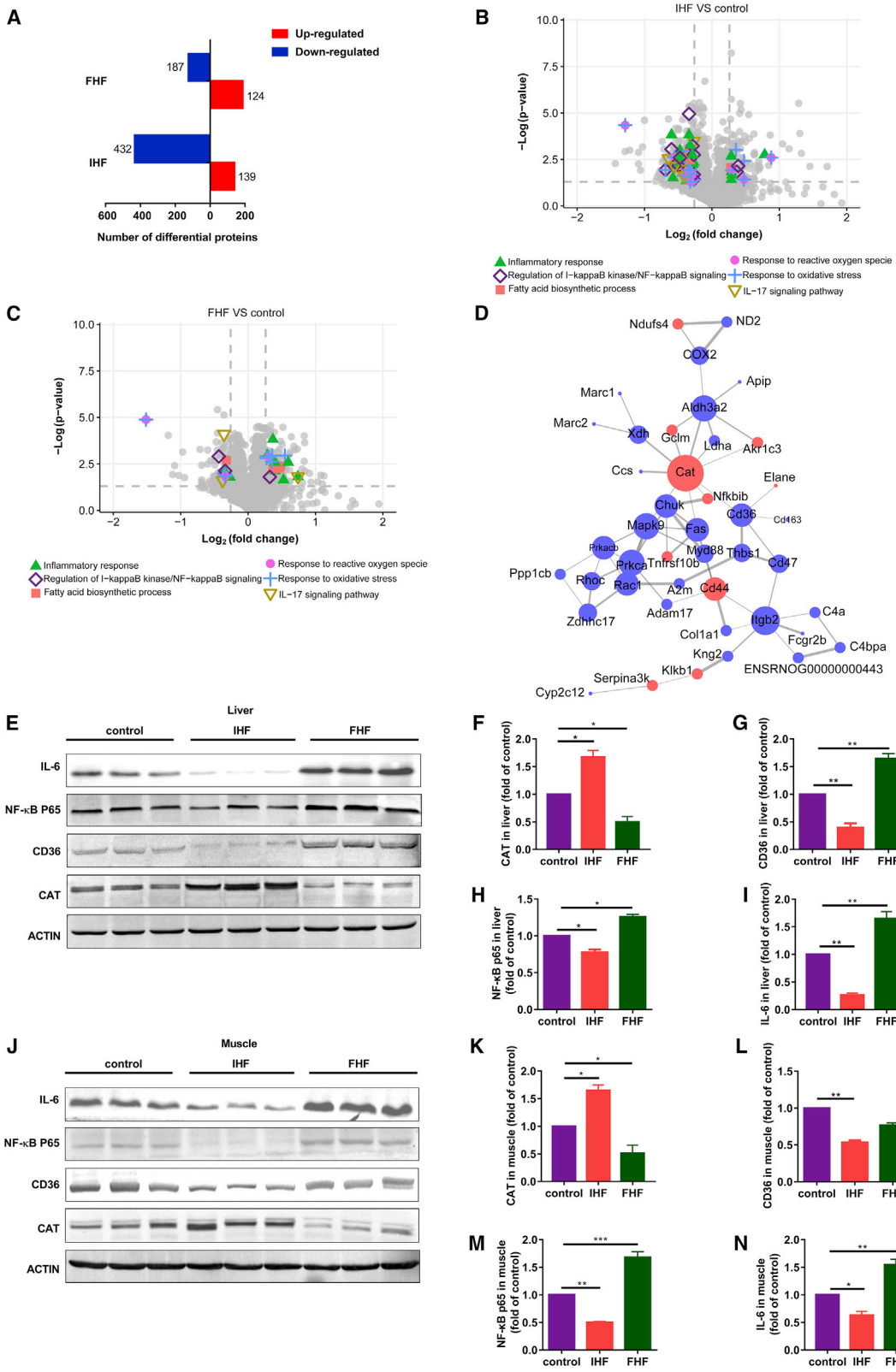


**Figure 4. Liver proteomic changes further reflect the improvement of oxidative stress, inflammation, and total FFA metabolism upon IHF**

(A) Protein expression changes in the liver, defined permissively for subsequent pathway analysis (fold change > 1.2, $p < 0.05$).

(B) KEGG and GO analysis for differential pathways between IHF and control.

*(legend continued on next page)*

stress and inflammation upon IHF, as assessed by upregulating the mRNA expression of cat and downregulating the mRNA expression of dorsal (Figure 6M), despite no change in crq. Taken together, these results indicate that decreased PA contributes to IHF-mediated lifespan extension by upregulating *Drosophila* homologous PPRC1.

### Decreased PA upregulates PPRC1, contributing to IHF-mediated changes in lifespan, oxidative stress, and inflammation through PPARG

To elucidate how PA regulated PPRC1, a bioinformatics analysis was performed, suggesting that PPARG, a protein involved in fatty acid metabolism, may mediate the effect of PA on the expression of PPRC1. In human hepatocyte (HepG2) cells, we demonstrated that exposure to PA significantly decreased PPRC1 and PPARG expression in a dose-dependent manner (Figures 7A–7C), while PPARG overexpression with the pharmacologic rosiglitazone (RGZ) approach increased the expression of PPRC1 in cells exposed to PA (Figures 7D–7F). In addition, 24 h exposure to PA increased the levels of ROS and IL-6 in a dose-dependent manner (Figures S5A and S5B). Correspondingly, PPRC1 and PPARG activation showed decreased levels of ROS and IL-6 in PA-treated cells, while PPRC1 siRNA silencing led to significant enhancement of oxidative stress and inflammation in cells without PA intervention (Figures 7G–7J, S5C, and S5D). Moreover, PPRC1 siRNA interference counteracted the inhibitory effect of RGZ on ROS and IL-6 elevation in cells treated with PA (Figures 7K and 7L). These results indicate that PA induces oxidative stress and inflammation by negatively regulating PPARG /PPRC1.

Next, we overexpressed Eip75B, the *Drosophila* homologous PPARG (dh-PPARG), using transgenic fly to measure the effect of dh-PPARG on lifespan and healthspan in flies raised on an IHF+PA. dh-PPARG overexpression flies partially restored the lifespan impairment in flies reared on PA in response to the IHF (Figure 7M), paralleled by a suppression of oxidative stress and inflammatory response with upregulated mRNA expression of cat as well as downregulated mRNA expression of crq and dorsal (Figure 7N). Next, we further measured the mRNA expression of dh-PPRC1 and found that it was also significantly more robust when dh-PPARG was upregulated (Figure 7N). Finally, the hepatic and muscular protein expression of PPARG in rats was persistently confirmed to be upregulated in the IHF group compared to the control group (Figures S5E–S5G). Taken together, the combined results suggest that decreased PA upregulates *Drosophila* homologous PPARG/PPRC1, contributing to IHF-mediated changes in lifespan, oxidative stress, and inflammation.

### PPARG/PPRC1 inversely correlates with age detected by human liver

Finally, we evaluated the association of hepatic PPARG/PPRC1 with age in human subjects. We found that the mRNA expression of PPARG was strongly inversely correlated with age in the liver tissue of humans, and the same was true for PPRC1 mRNA expression (Figure 7O). Moreover, our correlation analysis further revealed that PPARG and PPRC1 were negatively correlated with the levels of ROS, total FFAs and PA, but no change in IL-6 (Figures 7P and 7Q), in human liver tissues, which implies that PPARG could be a potential therapeutic target in diseases related to aging and oxidation stress.

### Beta-hydroxybutyrate is a secondary contributor to the IHF-mediated reduction in oxidative stress and inflammation in rats

Beta-hydroxybutyrate (BHB) is intrinsically produced in the context of dietary restriction, fasting, or extreme high-fat diets that result in extended longevity, decreased oxidative stress, and improved inflammation (Mattson et al., 2017; Newman et al., 2017; Youm et al., 2015). During the experiment, we found that the IHF significantly increased the serum content of BHB in rats (Figure S6A). However, it is still largely unknown whether BHB also mediates the effect of the IHF on the improvement of oxidative stress and inflammation. To elucidate this, we performed a 4-month experiment starting at 10 weeks of age in Wistar rats and intravenously injected the adeno-associated virus (AAV) of succinyl-CoA:3-ketoacid CoA transferase (SCOT), the main enzyme breaking down ketones to be used for energy, before the last 3 weeks to speed up BHB catabolism. The mRNA expression of SCOT in rats injected with the SCOT AAV was higher than that in the controls in liver, muscle, and heart tissues (Figure S6B). Some serum measures were changed, but most importantly, the total FFAs showed no change between the IHF and IHF+SCOT groups in the serum, liver, and muscle tissues, while total FFAs were still lower in the IHF+SCOT group than in the control+vehicle group (Figures S6C–S6F). Despite the results that the serum level of BHB was lower in the IHF+SCOT group than in the IHF group and was similar to that in the control+vehicle group (Figure S6G), the inflammatory marker IL-6 was still lower in the IHF+SCOT group than in the control+-vehicle group, although it displayed a significant increase in the IHF+SCOT group compared to the IHF group (FFA responsible for IL = 80.44%, BHB responsible for IL = 19.56%; Figure S6H). We also observed that ROS was nominally significantly decreased in the IHF+SCOT group compared to the control+-vehicle group ($p = 0.0656$; Figure S6I), but there was no difference between the IHF+SCOT and IHF groups (FFAs responsible for ROS = 94.49%, BHB responsible for ROS = 5.51%;

(C) KEGG and GO analysis for differential pathways between IHF and FHF.
(D) Protein-protein interaction analysis.
(E) Representative blots for oxidative stress and inflammation in the liver are shown for each protein. A representative loading control is shown for each case (n = 3).
(F–I) Quantification of (F) CAT, (G) CD36, (H) NF-κB p65, and (I) IL-6 protein levels.
(J) Representative blots for oxidative stress and inflammation in the muscle are shown for each protein. A representative loading control is shown for each case (n = 3).
(K–N) Quantification of (K) CAT, (L) CD36, (M) NF-κB p65, and (N) IL-6 protein levels.
Error bars, when present, show the SEM. *$p < 0.05$; **$p < 0.01$; ***$p < 0.001$; ****$p < 0.0001$. See also Figure S3 and Data S1 and S2.

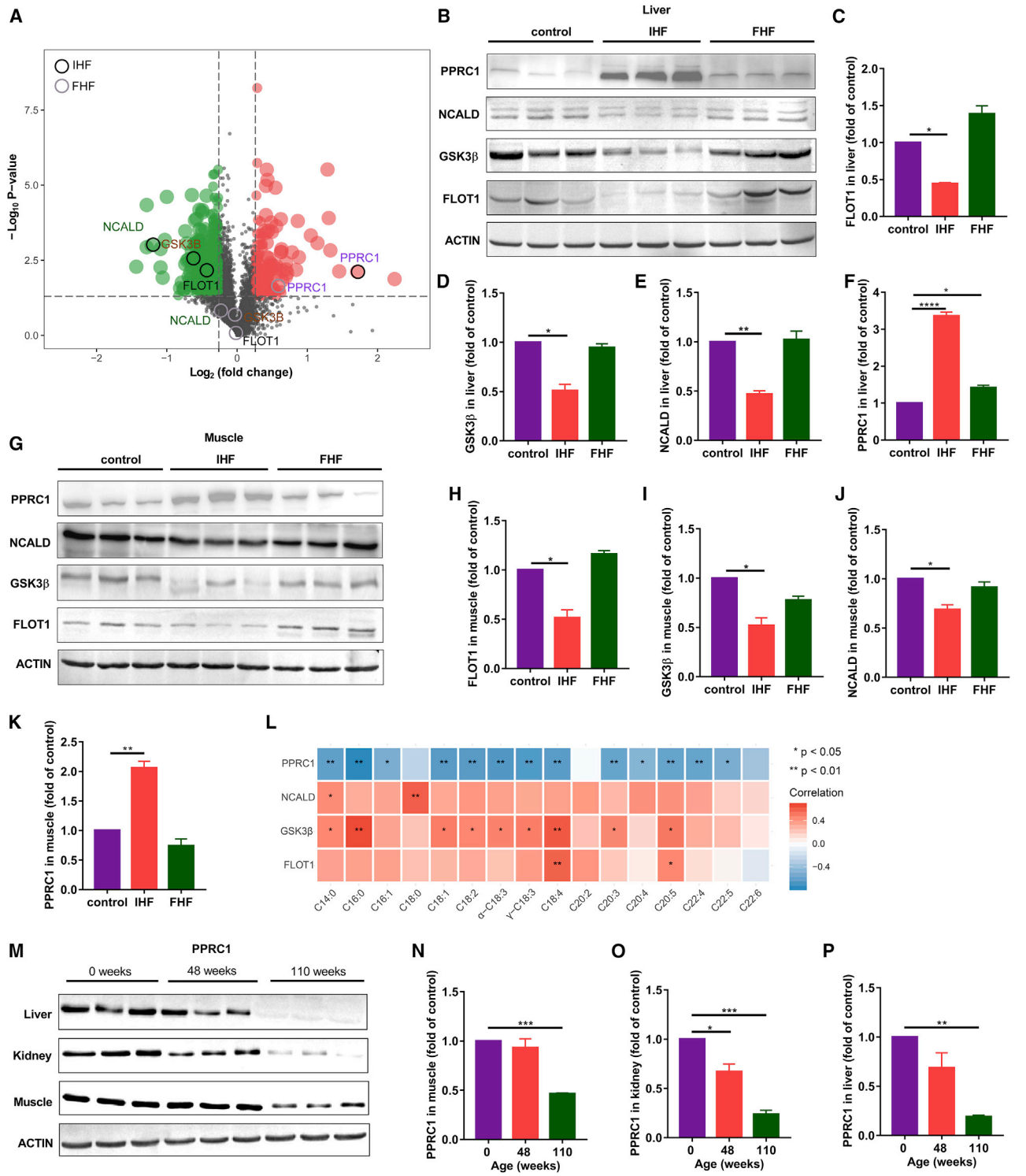


**Figure 5. Liver proteomic changes further identified PPRC1 as a candidate target**

(A) Volcano plot of the fold changes of proteins in response to the IHF or FHF diet in comparison with the control. Four candidate proteins selected for western blot confirmation are shown in different colors.

(B–F) Candidate protein levels in the liver were measured by western blot at 110 weeks.

(B) Representative blots are shown for each protein. A representative loading control is shown for each case (n = 3).

(C–F) Quantification of (C) FLOT1, (D) GSK-3β, (E) NCALD, and (F) PPRC1 protein levels.

(G–K) Candidate protein levels in the muscle were measured by western blot at 110 weeks.

*(legend continued on next page)*

Figure S6I), thus suggesting that FFAs rather than BHB in principle account for the inflammatory and oxidative stress status.

## Discussion

Dietary guidelines have long advocated to limit the dietary intake of total fat so as to maintain overall health, yet recent studies on the association between dietary fat and the risk of disease are controversial (Dehghan et al., 2017; Mozaffarian and Ludwig, 2015; Siri-Tarino et al., 2010; Wu et al., 2019). In this study, we investigated this issue using global examination methods, and a series of experiments were performed in rats and flies as well as *in vitro* to examine the health impact of a high-fat diet on lifespan by rigorously controlling energy intake. To the best of our knowledge, this study is the first to demonstrate that compared to a normal diet, an IHF diet promotes many aspects of health, with delayed tumor occurrence, preserved physical performance, and attenuated age-related pathological decline. Most importantly, an IHF diet prolongs the lifespan via decreased PA levels, which can upregulate the expression of PPARG/PPRC1, resulting in reduced oxidative stress and inflammation in rats and flies. Furthermore, a significant association between this pathway and aging has been demonstrated in human liver tissue. Moreover, this study demonstrates that decreased levels of PA rather than BHB primarily account for the ability of an IHF diet to reduce oxidative stress and inflammation.

Energy and protein intake may mediate the health effects of dietary interventions because energy restriction is a factor that strongly regulates aging, and protein restriction can extend lifespan in animal models (Fontana and Partridge, 2015; Mattison et al., 2012; Mirzaei et al., 2014; Piper and Bartke, 2008). Of note, there are regulatory compensatory feeding responses to dietary protein, and in that case, diet in higher protein alters food intake and then affects energy intake (Solon-Biet et al., 2014). In addition, previous studies have identified multiple micronutrients that affect healthy aging and are related to numerous poor outcomes, such as cancer, cardiovascular disease (CVD), diabetes, and all-cause mortality (Ames, 2018; Holick and Chen, 2008; Manson et al., 2019; Sinha-Hikim et al., 2011). In this study, we aimed to develop a rat diet with identical macronutrient (except for carbohydrate/fat), micronutrients, and energy intake values when adjusting food intake rather than a diet paradigm with contents of nutrients identical to those of a normal control diet. According to pilot study data in which an average 10.2% reduction in food intake was recorded after consumption of a high-fat diet that achieved an energy intake identical to that of the control, we developed an IHF diet with 10.2% more protein, minerals, vitamins, and cellulose in an attempt to keep the actual intake of these components identical to that in the control group. As a result, although the diets have different nutritional and micro nutritional compositions, we found that the absolute intake values of nutritional factors (casein, l-cystine, minerals, vitamins, and cellulose) and energy in the IHF group, on average, were similar to those in the control group, despite the average 11% reduction in food intake (Figure 1D; Table S4).

Our work also showed that compared with a control diet, an IHF diet delayed tumor occurrence, whereas an FHF diet did not induce tumor formation. Although previous studies have reported that a high-fat diet (minimum 45% energy from fat in most instances) could promote tumor formation, these studies were frequently conducted in animal tumor models (Beyaz et al., 2016; Kim et al., 2017; Labbé et al., 2019). However, the ability of a high-fat diet to induce spontaneous tumor formation in wild-type rodents may be different. Compared to controls, C57BL/6 males subjected to a high-fat diet did not show an increase in visible tumors on necropsy (Newman et al., 2017). Similarly, a statistically significant decrease in the incidence of spontaneous tumors in the high-fat group was observed in adenoma of the parathyroid gland in Wistar rats (Kristiansen et al., 1993). Our findings are in line with these studies, which also showed that compared with a regular diet, an FHF diet did not significantly induce spontaneous tumor formation.

Notably, our results showed that an IHF diet reduced oxidative stress levels, inflammation, and FFA profiles. It was difficult to explain how the IHF diet reduced these deleterious factors based on the available evidence. Therefore, proteomic analysis of the liver was performed to elucidate the potential mechanisms underlying the above observations, and proteomic data revealed that the IHF diet could downregulate these pathways. Consistent with the results of the proteomic analysis, we also found that the IHF diet regulated the mRNA or protein expression of genes related to lipid synthesis, including ACC and FAS, and genes related to lipid oxidation, such as CPT1a (whd) and CPT2, in the liver or muscle tissue of flies or rats, implying that the IHF diet suppresses lipid accumulation by inhibiting lipogenesis and promoting lipid oxidation. In line with our observations, a few studies have also shown that under either isocaloric or time-restricted conditions, a high-fat diet inhibited fatty acid synthesis or promoted fatty acid oxidation, accompanied by decreases in the concentrations of several fatty acids (Hatori et al., 2012; Lundsgaard et al., 2019).

Many studies focusing on supplementation of individual fatty acids have demonstrated that fatty acid metabolism is crucial for regulating lifespan (Goudeau et al., 2011; Lee et al., 2015; O'Rourke et al., 2013; Qi et al., 2017; Ratnappan et al., 2014) and have identified the enzymes of fatty acid metabolism that are involved in lifespan regulation (Goudeau et al., 2011; Johnson and Stolzing, 2019; Pan et al., 2017; Shmookler Reis et al., 2011; Wang et al., 2008). For example, knockdown of the fatty acid desaturase fat-7 eliminated the longevity-promoting effect of H3K4me3 chromatin modification deficiency, and FAT-7 overexpression promoted longevity (Han et al., 2017). Extending the

(G) Representative blots are shown for each protein. A representative loading control is shown for each case (n = 3).
(H–K) Quantification of (H) FLOT1, (I) GSK-3β, (J) NCALD, and (K) PPRC1 protein levels.
(L) Pearson correlations between the mRNA expressions of candidate proteins and FFAs profiles in rats aged 68 weeks (n = 21 rats).
(M–P) Protein expression of PPRC1 was detected by western blot at a different time point in different tissues upon control.
(M) Representative blots are shown for each protein. A representative loading control is shown for each case (n = 3).
(N–P) Quantification of PPRC1 in (N) muscle, (O) kidney, and (P) liver.
Pearson correlation analysis test for (L). Error bars, when present, show the SEM. *p < 0.05; **p < 0.01; ***p < 0.001; ****p < 0.0001. See also Data S1.

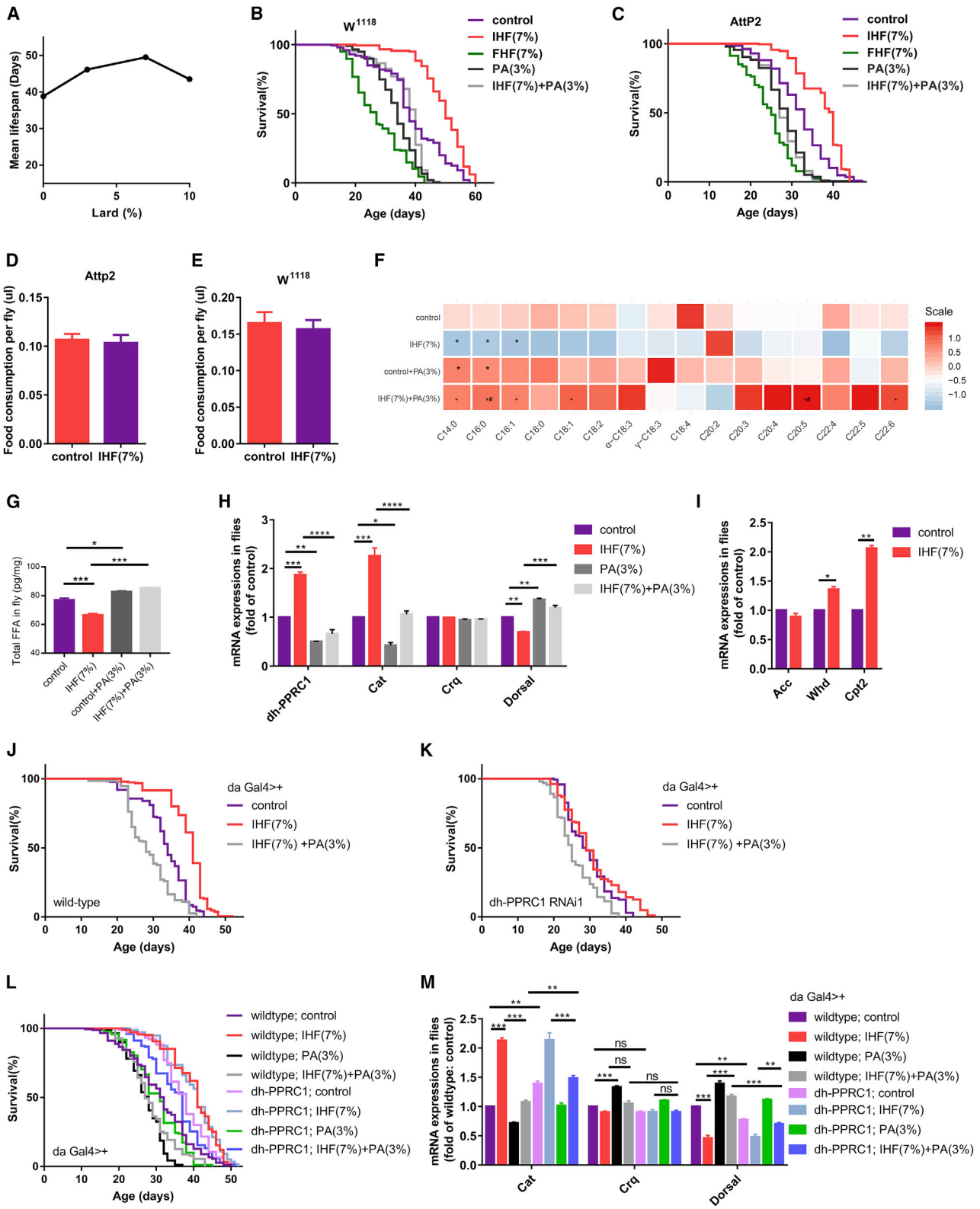


**Figure 6. Decreased PA upregulates PPRC1 involved in IHF-mediated change in lifespan, oxidative stress, and inflammation**

(A) $W^{1118}$ flies showed a stronger response to varying dietary lard concentrations under identical energy intake conditions.

(B) IHF extended lifespan of $w^{1118}$ male flies in intervention with PA or without PA ($p < 0.0001$ in either case, log-rank; n = 180–200 flies per group), but lifespan extension by IHF was reduced in intervention with PA (17.6%) compared to intervention without PA (31.6%) ($p < 0.0001$, two-way ANOVA).

*(legend continued on next page)*

previous studies, our study is the first to demonstrate the beneficial effect of an IHF diet on lifespan. We found that after consumption of the IHF diet, PA levels significantly decreased, which upregulated PPARG; dh-PPARG overexpression in flies further demonstrated that dh-PPARG was involved in the effect of decreased PA on IHF diet-mediated lifespan extension. These findings were supported by a series of previous studies. First, an increase in PA levels was found to be associated with accelerated aging, aging-related diseases, and shortened lifespan (Ford, 2010; Lee et al., 2015; Shmookler Reis et al., 2011). Second, it has been reported that PPARG, a classic regulator of fatty acid metabolism, is involved in aging and aging-related pathophysiological processes related to energy metabolism as well as inflammation (Erol, 2007; Hamaguchi and Sakaguchi, 2012; Zhang and Zheng, 2008); Argmann et al. also demonstrated that compared to wild-type controls, female Pparg2$^{-/-}$ mice showed a reduction in lifespan of approximately 8.8 weeks (Argmann et al., 2009).

Moreover, we found that PPRC1 displayed a conserved response to the IHF diet in rats and flies, with high expression levels, and a strong negative relation between PA levels and PPRC1 expression was also observed, which prompted us to conclude that PPRC1 probably played an important role in mediating the effect of decreased PA levels and increased PPARG levels on longevity in animals fed an IHF diet. Although a previous study reported that overexpression of the *Drosophila* homolog of PPRC1 could extend lifespan (Rera et al., 2011), it is still largely unknown whether PPRC1 is involved in the effect of an IHF diet on longevity. To examine this question, we performed a series of experiments *in vitro* and in flies. In the *in vitro* studies, we found that PA could directly and negatively regulate PPRC1 through PPARG, suggesting a link between fatty acid metabolism and PPRC1. In fly studies, dh-PPARG overexpression upregulated the mRNA expression of the *Drosophila* homolog of PPRC1, which further suggested that PPARG regulated the expression of PPRC1. On the background of a GAL4 driver line, PA impaired the ability of an IHF diet to extend lifespan in both wild-type flies and dh-PPRC1 RNAi1 mutants, but the lifespan impairment driven by PA in response to an IHF in wild-type flies (31.7%) was larger than that in dh-PPRC1 RNAi1 mutants (13.8%), demonstrating that PPRC1 primarily contributes to the mechanism by which an IHF diet decreased PA to extend lifespan, which was further supported by our findings in dh-PPRC1-overexpressing flies. It is important to note that *Drosophila* lacking a homolog of PPRC1 still displays some lifespan impairment, suggesting that PPRC1-independent pathways may contribute to the response to an IHF diet. This is not surprising, as multiple pathways are likely to function coordinately to mediate diet-driven lifespan extension (Fontana and Partridge, 2015; Papsdorf and Brunet, 2019). Overall, our data represent the first report that PA and PPARG regulate PPRC1 and its causative role in lifespan changes in response to an IHF diet.

A ketogenic diet, which typically contains an extremely large amount of energy from fat is one means of delivering high levels of BHB. Recently, ketogenic diets were shown to significantly reduce midlife mortality and improve the healthspan of mice, as well as to decrease oxidative stress and inflammation (Mattson et al., 2017; Newman et al., 2017; Roberts et al., 2018; Shimazu et al., 2013; Youm et al., 2015). Although we found that an IHF diet significantly increased the serum content of BHB in rats, unlike a ketogenic diet, we demonstrated that decreased PA levels rather than BHB primarily accounted for the effect of an IHF diet on improved oxidative stress and inflammation. However, further studies are needed to investigate the long-term effect of BHB on survival in response to an IHF diet.

## Conclusions

In conclusion, our longevity results provide evidence for the relationship between dietary fat and survival in both rats and *Drosophila* and suggest that to attain the maximal benefits of an IHF diet, rigorous control of energy intake is needed to reduce PA concentrations and promote improvements in oxidative stress and inflammation. More studies are needed to further investigate the mechanisms underlying IHF diet-mediated improvements and to optimize diet composition and feeding approaches to extend lifespan.

## Limitations of study

Although this study demonstrated that an IHF diet significantly prolonged lifespan, it also had certain limitations. First, to ensure the energy intake between the control and the IHF was identical, energy intake was measured every day as the basis for the next day's amount of food provided for the IHF group, but the body weight that was used to account for the individual differences of the rats with respect to body size, appetite, and energy

(C) IHF extended lifespan of attp2 male flies in intervention without PA, but not in intervention with PA ($p < 0.0001$ and $p = 0.3314$, respectively, log-rank test; n = 194–228 flies per group).
(D and E) Food intake was measured by the capillary feeder (CAFE) method for (D) w$^{1118}$ and (E) Attp2 (n = 20 flies per group, 11 days, male).
(F and G) IHF had a lowering effect on (F) FFA profiles and (G) total FFA concentration in w$^{1118}$ flies (200 mg flies per group). *Compared to control, $p < 0.05$; $^{+}$compared to IHF (7%), $p < 0.05$; $^{\#}$compared to control+ PA (3%), $p < 0.05$.
(H and I) mRNA expressions were measured by qRT-PCR in the whole body of flies. (H) Left, dh-PPRC1; left middle, cat; right middle, crq; right, dorsal. (I) Left, acc; middle, whd; right, cpt2 (n = 50 mg flies per group, 11 days, male).
(J and K) IHF extended lifespan in both wild-type flies and dh-PPRC1 RNAi1 mutants driven by daGal4 ($p < 0.0001$ and $p = 0.0173$, respectively, log-rank test; n = 168–194 flies per group), but lifespan extension upon IHF in (J) wild-type flies (20.6%) was larger than that in (K) dh-PPRC1 RNAi1 mutants (1.8%) ($p < 0.0001$, two-way ANOVA). PA impaired IHF-mediated lifespan extension in both wild-type flies and dh-PPRC1 RNAi1 mutants driven by daGal4 ($p < 0.0001$ for all comparison, log-rank test; n = 183–194 flies per group), but lifespan impairment driven by PA upon IHF in (J) wild-type flies (31.7%) was larger than that in (K) dh-PPRC1 RNAi1 mutants (13.8%) ($p < 0.0001$, two-way ANOVA).
(L) PA impaired IHF-mediated lifespan extension in both wild-type flies and dh-PPRC1-overexpressing flies ($p < 0.0001$ for all comparison, log-rank test), but lifespan impairment driven by PA upon IHF in wild-type flies (34.1%) was larger than that in flies with dh-PPRC1 overexpression (9.8%) ($p < 0.0001$, two-way ANOVA) (n = 160–182 flies per group).
(M) mRNA expression in the whole body of flies was measured by qRT-PCR. Left, cat; middle, crq; right, dorsal (n = 50 mg flies per group, 11 days, male).
Error bars, when present, show the SEM. *$p < 0.05$; **$p < 0.01$; ***$p < 0.001$; ****$p < 0.0001$. See also Figure S4 and Data S3.

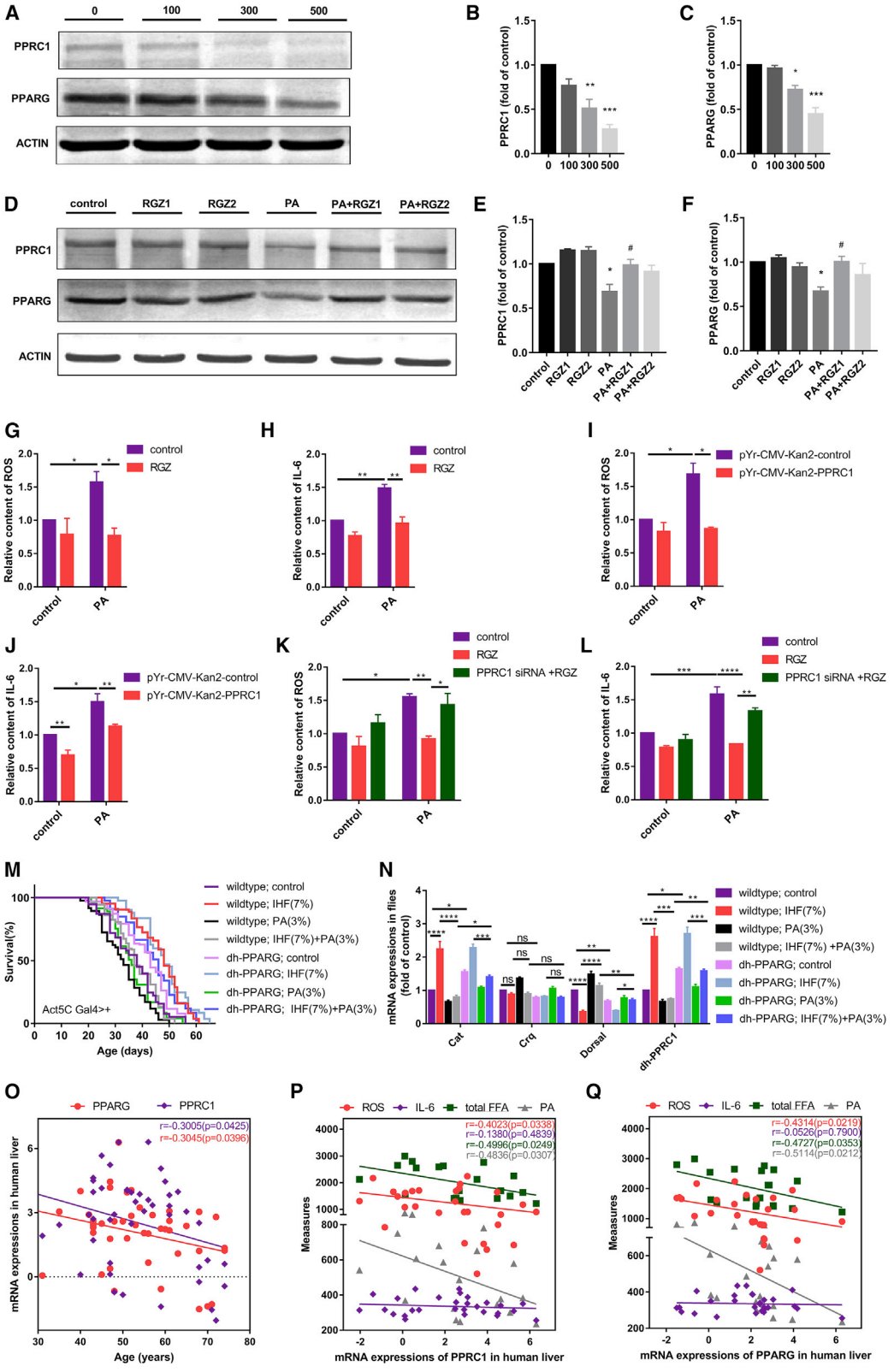


*(legend on next page)*

expenditure was monitored biweekly, it would be more accurate if the bodyweight was measured daily; however, abundant previous studies have shown that the bodyweight of adult rats gradually increased, whereas their daily energy intake steadily fluctuated within limits (Iwasa et al., 2018; Liu et al., 2015; Wang et al., 2007). Based on this evidence, when we designed our feeding paradigm, we thought that, to ensure the energy intake between the control and the IHF was identical, the most important factor was the average daily energy intake of the control group. Further, the trajectories of body weight for each animal showed that the growth curve was slow and stable in the IHF, no obvious fluctuations were observed, which indicated that the food supply for the IHF rats was adequate, and the measurement of body weight biweekly could largely reflect the body size, appetite, and energy expenditure for each rat in the IHF. Second, although our feeding paradigm could largely ensure the energy intake between the two groups identical and reflect the individual difference of each rat throughout the intervention of 770 days, this study could not make sure that the energy intake of every rat in every day was identical because there is still no way to perfectly control the food intake, leftover, and spillage of rats. Future study with rigorously controlling these factors is still needed to validate the findings in this study. Moreover, the experiment was carried out on animals of one sex (male). Reports have shown that numerous experimental variables alter longevity alterations in response to diet (Mitchell et al., 2016). Thus, further studies are warranted to address the effect of sex on survival and healthspan. Finally, although we observed all *Drosophila* postmortem, we did not observe all animal postmortems in the rat experiment. Although the median lifespan has been broadly used to reflect survival in lifespan investigations (Niu et al., 2013), additional works need to focus on detailed lifetime trajectories to detect the maximum lifespan in murine models. However, our findings still provide new insight into the provision of a large amount of energy from fat when controlling energy intake, which is indeed conducive to health.

## STAR★methods

Detailed methods are provided in the online version of this paper and include the following:

- KEY RESOURCES TABLE
- RESOURCE AVAILABILITY
  - Lead contact
  - Materials availability
  - Data and code availability
- EXPERIMENTAL MODEL AND SUBJECT DETAILS
  - Animals and diets
  - Drosophila stocks
  - Cell culture and treatment
  - Liver sample collection in humans
- METHOD DETAILS
  - Physical performance tests
  - Collection of blood and tissue
  - Indirect calorimetry
  - Proteomics analysis
  - Bioinformatics pipeline
  - Protein quantification
  - Western blot analysis
  - Quantitative real-time PCR
  - Food intake measurement in Drosophila
- QUANTIFICATION AND STATISTICAL ANALYSIS
  - Survival assessment
  - Pathology examinations and quantification
  - Blood chemistry measurement
  - Free fatty acids measurement
  - Blood beta-hydroxybutyrate levels
  - Statistical analysis

### Supplemental information

Supplemental Information can be found online at https://doi.org/10.1016/j.cmet.2020.12.017.

**Figure 7. Decreased PA upregulates PPRC1, contributing to IHF-dependent changes in lifespan, oxidative stress, and inflammation through PPARG**

(A–C) Protein expression at different PA concentrations was detected by western blot in hepatocyte (HepG2) cells.
(A) Representative blots are shown for each protein. A representative loading control is shown for each case.
(B and C) Quantification of (B) PPRC1 and (C) PPARG. *Compared with 0 mM PA, $p < 0.05$; **$p < 0.01$; ***$p < 0.001$.
(D–F) Protein expression of PPRC1 and PPARG in HepG2 cells exposed to PA and treated with RGZ, as analyzed by western blot.
(D) Representative blots are shown for each protein. A representative loading control is shown for each case.
(E and F) Quantification of (E) PPRC1 and (F) PPARG. *Compared with control, $p < 0.05$; **$p < 0.01$; #Compared with PA, $p < 0.05$; ##$p < 0.01$.
(G) ROS levels in HepG2 cells exposed to PA and treated with RGZ (n = 3–4).
(H) IL-6 levels in HepG2 cells exposed to PA and treated with RGZ (n = 3–4).
(I) ROS levels in HepG2 cells exposed to PA and transfected with pYr-CMV-Kan2-PPRC1 (n = 3).
(J) IL-6 levels in HepG2 cells exposed to PA and transfected with pYr-CMV-Kan2-PPRC1 (n = 3–4).
(K) ROS levels in HepG2 cells exposed to PA and cotransfected with PPRC1 siRNA and RGZ (n = 3–4).
(L) IL-6 levels in HepG2 cells exposed to PA and cotransfected with PPRC1 siRNA and RGZ (n = 3).
(M) PA impaired IHF-mediated lifespan extension in both wild-type flies and dh-PPARG-overexpressing flies ($p < 0.0001$ and $p = 0.0001$, respectively, log-rank test), but lifespan impairment driven by PA upon IHF in wild-type flies (22.9%) was larger than that in flies with dh-PPARG overexpression (4.2%) ($p < 0.0001$, two-way ANOVA) (n = 164–171 flies per group).
(N) mRNA expression in the whole body of flies was measured by qRT-PCR. Left, cat; left middle, crq; right middle, dorsal; right, dh-PPRC1 (n = 50 mg flies per group, 11 days, male).
(O–Q) Pearson correlations between serum measures, age, and PPARG/PPRC1 were conducted for human subjects (n = 46).
(O) Pearson correlations between age and mRNA expression of PPARG and PPRC1.
(P) Pearson correlations between mRNA expression of PPRC1 and serum parameters related to ROS, IL-6, total FFA, and PA.
(Q) Pearson correlations between mRNA expressions of PPARG and serum parameters related to ROS, IL-6, total FFA, and PA.
Error bars, when present, show the SEM. *$p < 0.05$; **$p < 0.01$; ***$p < 0.001$; ****$p < 0.0001$. See also Figure S5 and Data S3.

## Acknowledgments

This work was funded by the National Key R&D Program of China (2017YFC1307401), the National Natural Science Foundation of China (no. 82030100 to Y.L., no. 81673152 to Y.N., and no.81803227 to T.H.), the Postdoctoral Fund of Heilongjiang Province (LBH-Q17091), and the Young Elite Scientists Sponsorship Program by CAST (2019QNRC001).

## Author contributions

Conceptualization, C.S., Y.L., and Y.N.; Data curation, C.S., Y.L., and Y.N.; Methodology, C.S., Y.L., Y.N., D.S., and T.H.; Software, D.S. and T.H.; Visualization, C.S., Y.L., D.S., and T.H.; Formal Analysis, all authors; Investigation, D.S. (lifespan study); X.C., H.L., and X.Y. (cell experiment, western blot, and qPCRs); T.Z. and Y.Z. (pathological examination and metabolomic experiment); X.W., Z.L., J.R., and X.L. (lifespan study and short-term animal study); H.L., X.C., H.N., M.W., and Y.S. (biochemical assays); and Y.L., Y.W., F.L., and Y.G. (healthspan testing); Project administration, C.S, Y.L., and Y.N.; Resources, C.S., Y.L., Y.N., and D.S.; Validation, X.C., H.L., X.Y., Z.T., W.W., and R.G.; Writing – Original Draft, C.S., Y.L., and D.S.; Writing – Review & Editing, C.S., Y.L., Y.N., D.S., and T.H.; Supervision, Y.L. and Y.N.; Funding Acquisition, C.S., Y.L., Y.N., and T.H.

## Declaration of interests

The authors declare no competing interests.

Received: March 11, 2020
Revised: October 13, 2020
Accepted: December 21, 2020
Published: January 12, 2021

## References

Abumrad, N.A., and Goldberg, I.J. (2016). CD36 actions in the heart: lipids, calcium, inflammation, repair and more? Biochim. Biophys. Acta *1861*, 1442–1449.

Ames, B.N. (2018). Prolonging healthy aging: longevity vitamins and proteins. Proc. Natl. Acad. Sci. USA *115*, 10836–10844.

Argmann, C., Dobrin, R., Heikkinen, S., Auburtin, A., Pouilly, L., Cock, T.A., Koutnikova, H., Zhu, J., Schadt, E.E., and Auwerx, J. (2009). PPARgamma2 is a key driver of longevity in the mouse. PLoS Genet. *5*, e1000752.

Beyaz, S., Mana, M.D., Roper, J., Kedrin, D., Saadatpour, A., Hong, S.J., Bauer-Rowe, K.E., Xifaras, M.E., Akkad, A., Arias, E., et al. (2016). High-fat diet enhances stemness and tumorigenicity of intestinal progenitors. Nature *531*, 53–58.

Bonadonna, R.C., Groop, L.C., Simonson, D.C., and DeFronzo, R.A. (1994). Free fatty acid and glucose metabolism in human aging: evidence for operation of the Randle cycle. Am. J. Physiol. *266*, E501–E509.

Chen, Q., Niu, Y., Zhang, R., Guo, H., Gao, Y., Li, Y., and Liu, R. (2010). The toxic influence of paraquat on hippocampus of mice: involvement of oxidative stress. Neurotoxicology *31*, 310–316.

Da Mesquita, S., Louveau, A., Vaccari, A., Smirnov, I., Cornelison, R.C., Kingsmore, K.M., Contarino, C., Onengut-Gumuscu, S., Farber, E., Raper, D., et al. (2018). Functional aspects of meningeal lymphatics in ageing and Alzheimer's disease. Nature *560*, 185–191.

DeClerck, Y.A. (2016). Fat, calories, and cancer. Cancer Res. *76*, 509–510.

Dehghan, M., Mente, A., Zhang, X., Swaminathan, S., Li, W., Mohan, V., Iqbal, R., Kumar, R., Wentzel-Viljoen, E., Rosengren, A., et al. (2017). Associations of fats and carbohydrate intake with cardiovascular disease and mortality in 18 countries from five continents (PURE): a prospective cohort study. Lancet *390*, 2050–2062.

Deutsch, E.W., Bandeira, N., Sharma, V., Perez-Riverol, Y., Carver, J.J., Kundu, D.J., García-Seisdedos, D., Jarnuczak, A.F., Hewapathirana, S., Pullman, B.S., et al. (2020). The ProteomeXchange Consortium in 2020: enabling 'big data' approaches in proteomics. Nucleic Acids Res. *48*, D1145–D1152.

Diegelmann, S., Jansen, A., Jois, S., Kastenholz, K., Velo Escarcena, L., Strudthoff, N., and Scholz, H. (2017). The capillary feeder assay measures food intake in Drosophila melanogaster. J. Vis. Exp. *121*, 55024.

Erol, A. (2007). The functions of PPARs in aging and longevity. PPAR Res. *2007*, 39654.

Feng, Z., Hanson, R.W., Berger, N.A., and Trubitsyn, A. (2016). Reprogramming of energy metabolism as a driver of aging. Oncotarget *7*, 15410–15420.

Fontana, L., and Partridge, L. (2015). Promoting health and longevity through diet: from model organisms to humans. Cell *161*, 106–118.

Fontana, L., Partridge, L., and Longo, V.D. (2010). Extending healthy life span–from yeast to humans. Science *328*, 321–326.

Ford, J.H. (2010). Saturated fatty acid metabolism is key link between cell division, cancer, and senescence in cellular and whole organism aging. Age (Dordr.) *32*, 231–237.

Goudeau, J., Bellemin, S., Toselli-Mollereau, E., Shamalnasab, M., Chen, Y., and Aguilaniu, H. (2011). Fatty acid desaturation links germ cell loss to longevity through NHR-80/HNF4 in C. elegans. PLoS Biol. *9*, e1000599.

Hamaguchi, M., and Sakaguchi, S. (2012). Regulatory T cells expressing PPAR-gamma control inflammation in obesity. Cell Metab. *16*, 4–6.

Han, S., Schroeder, E.A., Silva-García, C.G., Hebestreit, K., Mair, W.B., and Brunet, A. (2017). Mono-unsaturated fatty acids link H3K4me3 modifiers to C. elegans lifespan. Nature *544*, 185–190.

Hatori, M., Vollmers, C., Zarrinpar, A., DiTacchio, L., Bushong, E.A., Gill, S., Leblanc, M., Chaix, A., Joens, M., Fitzpatrick, J.A., et al. (2012). Time-restricted feeding without reducing caloric intake prevents metabolic diseases in mice fed a high-fat diet. Cell Metab. *15*, 848–860.

Hofmann, J.W., Zhao, X., De Cecco, M., Peterson, A.L., Pagliaroli, L., Manivannan, J., Hubbard, G.B., Ikeno, Y., Zhang, Y., Feng, B., et al. (2015). Reduced expression of MYC increases longevity and enhances healthspan. Cell *160*, 477–488.

Holick, M.F., and Chen, T.C. (2008). Vitamin D deficiency: a worldwide problem with health consequences. Am. J. Clin. Nutr. *87*, 1080S–1086S.

Inoguchi, T., Li, P., Umeda, F., Yu, H.Y., Kakimoto, M., Imamura, M., Aoki, T., Etoh, T., Hashimoto, T., Naruse, M., et al. (2000). High glucose level and free fatty acid stimulate reactive oxygen species production through protein kinase C–dependent activation of NAD(P)H oxidase in cultured vascular cells. Diabetes *49*, 1939–1945.

Iwasa, T., Matsuzaki, T., Yano, K., and Irahara, M. (2018). The effects of ovariectomy and lifelong high-fat diet consumption on body weight, appetite, and lifespan in female rats. Horm. Behav. *97*, 25–30.

Johnson, A.A., and Stolzing, A. (2019). The role of lipid metabolism in aging, lifespan regulation, and age-related disease. Aging Cell *18*, e13048.

Kim, S., Yang, X., Li, Q., Wu, M., Costyn, L., Beharry, Z., Bartlett, M.G., and Cai, H. (2017). Myristoylation of Src kinase mediates Src-induced and high-fat diet-accelerated prostate tumor progression in mice. J. Biol. Chem. *292*, 18422–18433.

Kristiansen, E., Madsen, C., Meyer, O., Roswall, K., and Thorup, I. (1993). Effects of high-fat diet on incidence of spontaneous tumors in Wistar rats. Nutr. Cancer *19*, 99–110.

Labbé, D.P., Zadra, G., Yang, M., Reyes, J.M., Lin, C.Y., Cacciatore, S., Ebot, E.M., Creech, A.L., Giunchi, F., Fiorentino, M., et al. (2019). High-fat diet fuels prostate cancer progression by rewiring the metabolome and amplifying the MYC program. Nat. Commun. *10*, 4358.

Lee, D., Jeong, D.E., Son, H.G., Yamaoka, Y., Kim, H., Seo, K., Khan, A.A., Roh, T.-Y., Moon, D.W., Lee, Y., and Lee, S.-J.V. (2015). SREBP and MDT-15 protect C. elegans from glucose-induced accelerated aging by preventing accumulation of saturated fat. Genes Dev. *29*, 2490–2503.

Liu, A.G., Arceneaux, K.P., 3rd, Chu, J.T., Jacob, G., Jr., Schreiber, A.L., Tipton, R.C., Yu, Y., Johnson, W.D., Greenway, F.L., and Primeaux, S.D. (2015). The effect of caffeine and albuterol on body composition and metabolic rate. Obesity (Silver Spring) *23*, 1830–1835.

Liu, Z., Liu, R., Chou, J., Yu, J., Liu, X., Sun, C., Li, Y., and Liu, L. (2018). Targeted metabolomics analysis reveals the association between maternal

folic acid supplementation and fatty acids and amino acids profiles in rat pups. J. Chromatogr. B *1090*, 101–109.

Longo, V.D., Antebi, A., Bartke, A., Barzilai, N., Brown-Borg, H.M., Caruso, C., Curiel, T.J., de Cabo, R., Franceschi, C., Gems, D., et al. (2015). Interventions to slow aging in humans: are we ready? Aging Cell *14*, 497–510.

López-Otín, C., Blasco, M.A., Partridge, L., Serrano, M., and Kroemer, G. (2013). The hallmarks of aging. Cell *153*, 1194–1217.

Lundsgaard, A.M., Holm, J.B., Sjoberg, K.A., Bojsen-Moller, K.N., Myrmel, L.S., Fjaere, E., Jensen, B.A.H., Nicolaisen, T.S., Hingst, J.R., Hansen, S.L., et al. (2019). Mechanisms preserving insulin action during high dietary fat intake. Cell Metab. *29*, 50–63.e54.

Manson, J.E., Cook, N.R., Lee, I.M., Christen, W., Bassuk, S.S., Mora, S., Gibson, H., Gordon, D., Copeland, T., D'Agostino, D., et al. (2019). Vitamin D supplements and prevention of cancer and cardiovascular disease. N. Engl. J. Med. *380*, 33–44.

Martin-Montalvo, A., Mercken, E.M., Mitchell, S.J., Palacios, H.H., Mote, P.L., Scheibye-Knudsen, M., Gomes, A.P., Ward, T.M., Minor, R.K., Blouin, M.-J., et al. (2013). Metformin improves healthspan and lifespan in mice. Nat. Commun. *4*, 2192.

Mattison, J.A., Roth, G.S., Beasley, T.M., Tilmont, E.M., Handy, A.M., Herbert, R.L., Longo, D.L., Allison, D.B., Young, J.E., Bryant, M., et al. (2012). Impact of caloric restriction on health and survival in rhesus monkeys from the NIA study. Nature *489*, 318–321.

Mattson, M.P., Longo, V.D., and Harvie, M. (2017). Impact of intermittent fasting on health and disease processes. Ageing Res. Rev. *39*, 46–58.

Mirzaei, H., Suarez, J.A., and Longo, V.D. (2014). Protein and amino acid restriction, aging and disease: from yeast to humans. Trends Endocrinol. Metab. *25*, 558–566.

Mitchell, S.J., Madrigal-Matute, J., Scheibye-Knudsen, M., Fang, E., Aon, M., González-Reyes, J.A., Cortassa, S., Kaushik, S., Gonzalez-Freire, M., Patel, B., et al. (2016). Effects of sex, strain, and energy intake on hallmarks of aging in mice. Cell Metab. *23*, 1093–1112.

Mozaffarian, D., and Ludwig, D.S. (2015). The 2015 US dietary guidelines: lifting the ban on total dietary fat. JAMA *313*, 2421–2422.

Newman, J.C., Covarrubias, A.J., Zhao, M., Yu, X., Gut, P., Ng, C.P., Huang, Y., Haldar, S., and Verdin, E. (2017). Ketogenic diet reduces midlife mortality and improves memory in aging mice. Cell Metab. *26*, 547–557.e8.

Niu, Y., Na, L., Feng, R., Gong, L., Zhao, Y., Li, Q., Li, Y., and Sun, C. (2013). The phytochemical, EGCG, extends lifespan by reducing liver and kidney function damage and improving age-associated inflammation and oxidative stress in healthy rats. Aging Cell *12*, 1041–1049.

O'Rourke, E.J., Kuballa, P., Xavier, R., and Ruvkun, G. (2013). omega-6 polyunsaturated fatty acids extend life span through the activation of autophagy. Genes Dev. *27*, 429–440.

Pan, Y., Tian, T., Park, C.O., Lofftus, S.Y., Mei, S., Liu, X., Luo, C., O'Malley, J.T., Gehad, A., Teague, J.E., et al. (2017). Survival of tissue-resident memory T cells requires exogenous lipid uptake and metabolism. Nature *543*, 252–256.

Papsdorf, K., and Brunet, A. (2019). Linking lipid metabolism to chromatin regulation in aging. Trends Cell Biol. *29*, 97–116.

Pereira, S., Park, E., Mori, Y., Haber, C.A., Han, P., Uchida, T., Stavar, L., Oprescu, A.I., Koulajian, K., Ivovic, A., et al. (2014). FFA-induced hepatic insulin resistance in vivo is mediated by PKCδ, NADPH oxidase, and oxidative stress. Am. J. Physiol. Endocrinol. Metab. *307*, E34–E46.

Perez-Riverol, Y., Csordas, A., Bai, J., Bernal-Llinares, M., Hewapathirana, S., Kundu, D.J., Inuganti, A., Griss, J., Mayer, G., Eisenacher, M., et al. (2019). The PRIDE database and related tools and resources in 2019: improving support for quantification data. Nucleic Acids Res. *47*, D442–D450.

Piper, M.D.W., and Bartke, A. (2008). Diet and aging. Cell Metab. *8*, 99–104.

Qi, W., Gutierrez, G.E., Gao, X., Dixon, H., McDonough, J.A., Marini, A.M., and Fisher, A.L. (2017). The omega-3 fatty acid alpha-linolenic acid extends Caenorhabditis elegans lifespan via NHR-49/PPARalpha and oxidation to oxylipins. Aging Cell *16*, 1125–1135.

Ratnappan, R., Amrit, F.R., Chen, S.W., Gill, H., Holden, K., Ward, J., Yamamoto, K.R., Olsen, C.P., and Ghazi, A. (2014). Germline signals deploy NHR-49 to modulate fatty-acid beta-oxidation and desaturation in somatic tissues of C. elegans. PLoS Genet. *10*, e1004829.

Rera, M., Bahadorani, S., Cho, J., Koehler, C.L., Ulgherait, M., Hur, J.H., Ansari, W.S., Lo, T., Jr., Jones, D.L., and Walker, D.W. (2011). Modulation of longevity and tissue homeostasis by the Drosophila PGC-1 homolog. Cell Metab. *14*, 623–634.

Roberts, M.N., Wallace, M.A., Tomilov, A.A., Zhou, Z., Marcotte, G.R., Tran, D., Perez, G., Gutierrez-Casado, E., Koike, S., Knotts, T.A., et al. (2018). A ketogenic diet extends longevity and healthspan in adult mice. Cell Metab. *27*, 1156.

Schriner, S.E., and Linford, N.J. (2006). Extension of mouse lifespan by overexpression of catalase. Age (Dordr.) *28*, 209–218.

Sheedy, F.J., Grebe, A., Rayner, K.J., Kalantari, P., Ramkhelawon, B., Carpenter, S.B., Becker, C.E., Ediriweera, H.N., Mullick, A.E., Golenbock, D.T., et al. (2013). CD36 coordinates NLRP3 inflammasome activation by facilitating intracellular nucleation of soluble ligands into particulate ligands in sterile inflammation. Nat. Immunol. *14*, 812–820.

Shimazu, T., Hirschey, M.D., Newman, J., He, W., Shirakawa, K., Le Moan, N., Grueter, C.A., Lim, H., Saunders, L.R., Stevens, R.D., et al. (2013). Suppression of oxidative stress by β-hydroxybutyrate, an endogenous histone deacetylase inhibitor. Science *339*, 211–214.

Shmookler Reis, R.J., Xu, L., Lee, H., Chae, M., Thaden, J.J., Bharill, P., Tazearslan, C., Siegel, E., Alla, R., Zimniak, P., and Ayyadevara, S. (2011). Modulation of lipid biosynthesis contributes to stress resistance and longevity of C. elegans mutants. Aging *3*, 125–147.

Sinha-Hikim, I., Sinha-Hikim, A.P., Shen, R., Kim, H.J., French, S.W., Vaziri, N.D., Crum, A.C., Rajavashisth, T.B., and Norris, K.C. (2011). A novel cystine based antioxidant attenuates oxidative stress and hepatic steatosis in diet-induced obese mice. Exp. Mol. Pathol. *91*, 419–428.

Siri-Tarino, P.W., Sun, Q., Hu, F.B., and Krauss, R.M. (2010). Meta-analysis of prospective cohort studies evaluating the association of saturated fat with cardiovascular disease. Am. J. Clin. Nutr. *91*, 535–546.

Solon-Biet, S.M., McMahon, A.C., Ballard, J.W.O., Ruohonen, K., Wu, L.E., Cogger, V.C., Warren, A., Huang, X., Pichaud, N., Melvin, R.G., et al. (2014). The ratio of macronutrients, not caloric intake, dictates cardiometabolic health, aging, and longevity in ad libitum-Fed Mice. Cell Metab. *31*, 654.

Tripathy, D., Mohanty, P., Dhindsa, S., Syed, T., Ghanim, H., Aljada, A., and Dandona, P. (2003). Elevation of free fatty acids induces inflammation and impairs vascular reactivity in healthy subjects. Diabetes *52*, 2882–2887.

Wang, C., Yang, N., Wu, S., Liu, L., Sun, X., and Nie, S. (2007). Difference of NPY and its receptor gene expressions between obesity and obesity-resistant rats in response to high-fat diet. Horm. Metab. Res. *39*, 262–267.

Wang, M.C., O'Rourke, E.J., and Ruvkun, G. (2008). Fat metabolism links germline stem cells and longevity in C. elegans. Science *322*, 957–960.

Wen, B., Zhou, R., Feng, Q., Wang, Q., Wang, J., and Liu, S. (2014). IQuant: an automated pipeline for quantitative proteomics based upon isobaric tags. Proteomics *14*, 2280–2285.

Wu, J.H.Y., Micha, R., and Mozaffarian, D. (2019). Dietary fats and cardiometabolic disease: mechanisms and effects on risk factors and outcomes. Nat. Rev. Cardiol. *16*, 581–601.

Xie, K., Neff, F., Markert, A., Rozman, J., Aguilar-Pimentel, J.A., Amarie, O.V., Becker, L., Brommage, R., Garrett, L., Henzel, K.S., et al. (2017). Every-other-day feeding extends lifespan but fails to delay many symptoms of aging in mice. Nat. Commun. *8*, 155.

Youm, Y.H., Nguyen, K.Y., Grant, R.W., Goldberg, E.L., Bodogai, M., Kim, D., D'Agostino, D., Planavsky, N., Lupfer, C., Kanneganti, T.D., et al. (2015). The ketone metabolite beta-hydroxybutyrate blocks NLRP3 inflammasome-mediated inflammatory disease. Nat. Med. *21*, 263–269.

Zhang, R., and Zheng, F. (2008). PPAR-gamma and aging: one link through klotho? Kidney Int. *74*, 702–704.

## STAR★methods

### Key resources table

| REAGENT or RESOURCE | SOURCE | IDENTIFIER |
|---|---|---|
| Antibodies | | |
| Rabbit monoclonal Anti-Flotillin-1 | Cell Signaling Technology | Cat# 18634; RRID: AB_277304081 |
| Rabbit Anti-Fatty Acid Synthase | Cell Signaling Technology | Cat# 3180; RRID: AB_2100796 |
| Rabbit monoclonal Anti-Catalase | Cell Signaling Technology | Cat# 14097; RRID: AB_2798391 |
| Rabbit monoclonal Anti-GSK-3β | Cell Signaling Technology | Cat# 12456; RRID: AB_26369787 |
| Rabbit polyclonal Anti-Acetyl-CoA Carboxylase | Cell Signaling Technology | Cat# 3676; RRID: AB_2219397 |
| Mouse monoclonal Anti-β-Actin | Cell Signaling Technology | Cat# 58169; RRID: AB_2750839 |
| Rabbit polyclonal Anti-CD36 | Abcam | Cat# ab80978; RRID: AB_1640333 |
| Rabbit polyclonal Anti-NCALD | Absin Bioscience | Abs139207 |
| Mouse polyclonal Anti-CPTII | Santa Cruz Biotechnology | Sc-377294 |
| Rabbit polyclonal Anti-NFκB p65 | WanLeiBio | WL 01273b |
| Anti-IL6 Rabbit pAb | WanLeiBio | WL02841 |
| Mouse monoclonal Anti-CPT1A | Abcam | Cat# ab128568; RRID: AB_11141632 |
| Rabbit monoclonal Anti-PPARγ | Cell Signaling Technology | Cat# 2443; RRID: AB_823598 |
| Rabbit monoclonal Anti-PPARγ | WanLeiBio | WL01800 |
| Mouse monoclonal Anti-PPRC1 | Santa Cruz Biotechnology | Cat# sc-376431; RRID: AB_11149017 |
| Rabbit polyclonal Anti-PPRC1 | OriGene Technologies | Cat# AP53426PU-N; RRID: AB_11145429 |
| Anti-Rabbit IgG (Fc), AP Conjugate | Promega | Cat# S3731; RRID: AB_430872 |
| Anti-Mouse IgG (H+L), AP Conjugate | Promega | Cat# S3721; RRID: AB_430871 |
| Chemicals, peptides, and recombinant proteins | | |
| Control diet (custom) | N/A | See Table S1 |
| IHF diet (custom) | N/A | See Table S1 |
| FHF diet (custom) | N/A | See Table S1 |
| Palmitic acid | Sigma-Aldrich | P5585 |
| Lipofectamine 2000 Reagent | Invitrogen | Cat#11668027 |
| pYr-CMV-Kan2-PPRC1 | Yingrun Biotechnology | HO015062 |
| pYr-CMV-Kan2-control | Yingrun Biotechnology | N/A |
| PPRC1 siRNA | Santa Cruz Biotechnology | Sc-90572 |
| Control siRNA-A | Santa Cruz Biotechnology | Sc-37007 |
| Rosiglitazone | MedChemExpress LLC | CAS#122320-73-4 |
| Pioglitazone | MedChemExpress LLC | CAS#111025-46-8 |
| TRIzol reagent | Invitrogen | Cat#15596026 |
| RIPA lysis buffer | Beyotime | P0013C |
| Phenylmethanesulfonyl fluoride (PMSF) | Beyotime | ST506 |
| Trypsin Gold, Mass Spectrometry Grade | Promega | V5280 |
| Rat ACTB Endogenous Reference Genes Primers | Sangon Biotech | B661202-0001 |
| Human ACTB Endogenous Reference Genes Primers | Sangon Biotech | B661102-0001 |
| Critical commercial assays | | |
| Human IL-6 ELISA | Lengton Bioscience | BPE10140 |
| Human ROS ELISA | Lengton Bioscience | BPE11725 |

(*Continued on next page*)

*Continued*

| REAGENT or RESOURCE | SOURCE | IDENTIFIER |
|---|---|---|
| High-Capacity cDNA Reverse Transcription Kit | Applied Biosystems | 4374966 |
| Total Nitric Oxide Assay Kit | Beyotime | S0024 |
| GSH and GSSG Assay Kit | Beyotime | S0053 |
| Lipid Peroxidation MDA Assay Kit | Beyotime | S0131 |
| Total Superoxide Dismutase Assay | Beyotime | S0101 |
| Mouse/Rat Insulin ELISA Kit | Westang | N/A |
| Mouse/Rat IL-6 ELISA Kit | Biotopped | TOPEL02879 |
| Mouse/Rat TNF-α ELISA Kit | Biotopped | TOPEL02868 |
| Mouse/Rat ROS ELISA Kit | Biocompare | Abx156053 |
| Beta-hydroxybutyrate Assay Kit | Sigma-Aldrich | MAK041 |
| Deposited data | | |
| The proteomics data | This paper | Identifier: PXD022585 |
| Experimental models: cell lines | | |
| Human hepatocytes (HepG2) cells | Chinese Academy of Science | N/A |
| Experimental models: organisms/strains | | |
| Wistar rat | Vital River Laboratory Animal Technology Company LTD | N/A |
| $W^{1118}$ | Tsinghua Drosophila Stock Center | THJ0265 |
| Dh-PPRC1 RNAi-1 | Tsinghua Drosophila Stock Center | HMS00857 |
| Dh-PPRC1 RNAi-2 | Tsinghua Drosophila Stock Center | HMS00858 |
| Dh-PPRC1 overexpressions using flySAM Transgenic CRISPRa | Tsinghua Drosophila Stock Center | TH14666S |
| UAS-Eip75B overexpressions (genotype: w*; p {UAS-Eip75B} attP2/ TM6B) | Fungene Biotechnology | N/A |
| y[1] w[*]; P{w[+mC]=Act5C-GAL4} 25FO1/ CyO,y[+] | Fungene Biotechnology | N/A |
| Ubi-Gal4 | Tsinghua Drosophila Stock Center | TB00152 |
| Daughterless Gal4 | Tsinghua Drosophila Stock Center | TB00153 |
| Tub Gal4/TM6b, Tb | Tsinghua Drosophila Stock Center | TB00129 |
| y v; attP2, y+ | Tsinghua Drosophila Stock Center | TB00072 |
| Software and algorithms | | |
| Prism 7.0 | GraphPad | http://www.graphpad.com/scientific-software/prism; RRID: SCR_015807 |
| SPSS 17.0 | SPSS | 17.0 |
| R (version 3.5.1) | R | https://www.r-project.org/ |
| DAVID tool | DAVID | http://david.ncifcrf.gov/ |
| STRING | STRING | https://string-db.org/ |
| Cytoscape (version 3.6.1) | Cytoscape Consortium | https://cytoscape.org/ |
| Thermo Scientific Xcalibur 3.1 | Xcalibur | 3.1 |
| Other | | |
| Shuttle box tests | Taimeng | N/A |
| Morris water maze | Taimeng | N/A |
| Treadmill | Taimeng | N/A |
| ROCHE Modular P800 Biochemical Analyzer | Roche Diagnostics | N/A |
| The indirect calorimetry | TSE | N/A |
| Calibration capillary | VWR, West Chester, PA | #53432-706 |
| GC/MS-MS | Thermo Finnigan | N/A |

## Resource availability

### Lead contact

Further information and requests for resources and reagents should be directed to and will be fulfilled by the Lead Contact, Changhao Sun (changhaosun2002@163.com).

### Materials availability

This study did not generate new unique reagents.

### Data and code availability

The mass spectrometry proteomics data have been deposited to the ProteomeXchange Consortium via the PRIDE (Deutsch et al., 2020; Perez-Riverol et al., 2019) partner repository with the dataset identifier PXD022585. Original datasets of the results in this manuscript were deposited in the Data S1.

## Experimental model and subject details

### Animals and diets

Animals and diets for survival experiments: Male Wistar rats aged 8 weeks (n = 90) were purchased from Vital River Laboratory Animal Technology Company (Beijing, China) and were randomly assigned to the control, IHF or FHF group after three days of adaptation. All animals were housed in stainless steel individual cages and received their respective standard rodent chow diet paradigms in line with the group scheme for the entire study. A control diet matching the composition of the standard purified rodent diet AIN-93G was used in various animal studies. Notably, we developed the IHF ingredients to keep the protein and micronutrient intake identical to that in the control group according to pilot study data. Another group of FHF rodents were freely fed high-fat chow. Food paradigms of rats are as follows (g/kg):

| Component (g) | Control | IHF | FHF |
|---|---|---|---|
| Casein | 200.0 | 220.4 | 200.0 |
| L-cystine | 3.0 | 3.5 | 3.0 |
| Cornstarch | 397.5 | 304.5 | 325.5 |
| Dextrinized cornstarch | 132.0 | 114.4 | 114.0 |
| Sucrose | 100.0 | 80.0 | 88.0 |
| Soybean oil | 70.0 | 70.0 | 70.0 |
| Lard | 0.0 | 100.0 | 102.0 |
| Mixed minerals | 35.0 | 38.6 | 35.0 |
| Mixed vitamins | 10.0 | 11.0 | 10.0 |
| Cellulose | 50.0 | 55.1 | 50.0 |
| Choline | 2.5 | 2.5 | 2.5 |
| | 1000.0 | 1000.0 | 1000.0 |
| Energy from macronutrients (%) | | | |
| Carbohydrate | 63.6 | 45.1 | 47.2 |
| Protein | 20.5 | 20.3 | 18.2 |
| Fat | 15.9 | 34.6 | 34.6 |

To ensure that the control and IHF diets were isocaloric, every IHF animal was dynamically provided with different food allotments individually according to the average energy intake per gram of body weight for each rat in the control group. Specifically, each rat in the control group was provided with enough amount of food (40-50 g) every day, and after 24 hours we weighed the amount of unconsumed food, including food spillage on the plate and food leftover in the food box, respectively. The average daily food intake was computed by the amount of food supply minus the amount of unconsumed food. The average daily energy intake of the control group was calculated by the daily food intake × 3.96 (the energy density of the food in the control), and the average daily energy intake per gram of body weight in the control group was calculated: the average daily energy intake/ the average body weight. Accordingly, the daily energy intake of each rat in the IHF group was calculated by multiplying the average daily energy intake per gram of body weight in the control group by the weight of each IHF rat. Finally, the daily food supply to each IHF rat for the day was computed by [the daily energy intake of each rat / 4.385 (the energy density of food in the IHF)] + unconsumed food, which was recorded from the previous 24 hours in the IHF group. For the duration of the study, pellet chow was produced every 3 months and stored at -20°C until it was used to guarantee that the chow retained its original palatability. Body weight was

monitored biweekly in the morning. The rats were maintained under a 12 hour light/dark cycle in an environmentally controlled room at 21 ± 2°C and 50% ± 5% humidity under pathogen-free conditions. Daily energy intake, daily food intake and biweekly body weight for each single-housed rat was provided (Figure S7).

Short-term animal intervention: Male Wistar rats aged 10 weeks (n = 45) were purchased from Vital River Laboratory Animal Technology Company (Beijing, China). After 3 days of adaptive feeding, the rats were randomly divided into two groups according to their body weight: the control group and the IHF group. After three and a half months of feeding, the control group was randomly divided into two groups: the control group and the control+vehicle group. The IHF group was randomly divided into two groups: the IHF group and the IHF+SCOT group. Adeno-associated virus (AAV) was injected into the caudal vein, with the control+vehicle group being injected with blank control AAV and the IHF+SCOT group being injected with SCOT AAV (200 μl/per body weight). Three weeks after the injection, we ended the experiment. During the experiment, the amount of remaining feed and the amount of food scattered were recorded every other day. Body weight was monitored biweekly in the morning. The laboratory environment was the same as described in the experiment described above.

All protocols were approved by the Medical Ethics Committee of Harbin Medical University (Harbin, China) and were performed according to the Guide for Care and Use of Laboratory Animals.

## Drosophila stocks

The following Drosophila melanogaster strains were purchased from the Tsinghua Drosophila Stock Center (Beijing, China): $W^{1118}$ (THJ0265), y v; attP2, y+(y[1] v[1]; P{y[+t7.7]=CaryP}attP2 (TB00072), dh-PPRC1 RNAi-1 (HMS00857), dh-PPRC1 RNAi-2 (HMS00858), dh-PPRC1 overexpression using flySAM Transgenic CRISPRa (TH14666S), Ubi Gal4 (TB00152), Daughterless Gal4 (TB00153) and Tub Gal4/TM6b, Tb (TB00129). UAS-Eip75B overexpression lines (genotype: w*; p {UAS-Eip75B} attP2/ TM6B) and y[1] w[*]; P{w[+mC]=Act5C-GAL4}25FO1/CyO,y[+]) were purchased from Fungene Biotechnology (Jiangsu, China). All fly strains were housed in a fly incubator set at 25°C with 60% humidity under a 12-h light/dark cycle and were transferred to various types of media within 3 days of eclosion. For the survival experiment, mated males were maintained in fly vials (25-30 males/vial) and were transferred onto fresh medium within 3-4 days; deaths were recorded.

Recipes used for larval media and fly media for survival analyses are as follows (w/v):

| Component (g) | Larval media | Control (0%) | IHF (3%) | IHF (7%) | IHF (10%) |
|---|---|---|---|---|---|
| Agar | 10 | 11 | 11 | 11 | 11 |
| Dextrose | 55 | 145 | 103.53 | 48.29 | 1.52 |
| Corn meal | 60 | 50 | 50 | 50 | 50 |
| Sucrose | 30 | 91 | 64.97 | 30.3 | 9.56 |
| Yeast | 25 | 18 | 18 | 18 | 18 |
| 20% Tegosept | 15 | 15 | 15 | 15 | 15 |
| Propionic acid | 3 | 3 | 3 | 3 | 3 |
| Lard | 0 | 0 | 30 | 70 | 100 |
| Water | 1000ml | 1000ml | 1000ml | 1000ml | 1000ml |
| Calorie (cal) | | | | | |
| Carbohydrate | — | 1087.45 | 817.45 | 457.81 | 187.77 |
| Protein | — | 75.46 | 75.46 | 75.46 | 75.46 |
| Fat | — | 15.50 | 285.50 | 645.50 | 915.50 |
| Total calorie | — | 1178.402 | 1178.402 | 1178.762 | 1178.722 |

3% (w/v) PA media: The media recipe is applied to assay the response of flies to various concentrations of PA. The media type is same as 0% or 7% (w/v) fly media differing only in the amount of PA used.

7% (w/v) FHF media: The media type is adding 7% (w/v) lard on the basis of 0% (w/v) control lard media.

## Cell culture and treatment

Human hepatocytes (HepG2) obtained from the Chinese Academy of Science (Shanghai, China) were incubated at 37°C in a 5% $CO_2$ and 95% air atmosphere. To mimic the reduction of PPRC1 or PPARG expression caused by high levels of PA in vitro, we examined the expression of PPRC1 or PPARG at the mRNA and protein levels after 24 hours of treatment with gradient concentrations of PA (Sigma-Aldrich, Taufkirchen, Germany). To investigate the possible mechanism by which PA prolongs healthy life through PPRC1, we performed 24-hour fatty acid intervention on cells transfected and nontransfected with a PPRC1-overexpressing plasmid and then detected IL-6 and reactive oxygen species (ROS) (Lengton Bioscience, Shang Hai, China) according to the descriptions of the manuals. Specifically, the cells were transfected in 6-well plates using Lipofectamine 2000 Reagent (Invitrogen, Carlsbad, CA) by adding 1 μg of pYr-CMV-Kan2-PPRC1 or pYr-CMV-Kan2-control (Yingrun Biotechnology, Changsha, China) or 40 pmol of PPRC1 siRNA or

control siRNA-A (Santa Cruz Biotechnology, CA, USA) per well and incubated for 24 hours according to the instructions. Furthermore, when verifying the regulatory effect of PPARG on PPRC1 and its effect on the cellular inflammatory response, cells were pretreated with a 30 mmol/L concentration of the PPARG agonist rosiglitazone (MedChemExpress LLC) for 2 hours, and then IL-6 and ROS were detected with or without the addition of 300 mmol/L PA for 24 hours. Finally, to demonstrate that PPARG regulates IL-6 and ROS in part through PPRC1, PPARG was activated with 30 mmol/L RGZ, PPRC1 was inhibited by simultaneous transfection with 40 pmol per well of PPRC1 siRNA, and then IL-6 and ROS were detected after 24 hours of treatment.

### Liver sample collection in humans

Liver samples were collected from patients who underwent hepatic hemangioma surgery in the Department of Hepatobiliary and Pancreatic Surgery (Harbin Medical University Cancer Hospital, Harbin, China). This study included 46 patients aged 31 to 74 years old, including 25 men and 21 women. The study protocol was registered with the number ChiCTR1900021884 and was approved by the Human Research Ethics Committee of the hospital. Written informed consent was obtained from all patients.

### Method details

### Physical performance tests

Shuttle box (Taimeng, Chengdu, China), Morris water maze (Taimeng, Chengdu, China), and treadmill (Taimeng, Chengdu, China) tests were performed on young rats (n = 5-6 per group; age = 64 weeks) between 13:00 and 18:00. For the shuttle box test, the results of conditional responses and error response times were recorded. As described previously (Da Mesquita et al., 2018), animals that had adapted to the box for 5 min were trained for 5 consecutive days and tested on the 6th day. During the length of the experiment, the parameters were set as a 3 s conditional light stimulus and a 3 s unconditional electrical shock stimulus at 0.5–1.0 mA within a 30 s trial, with 20 trials per day.

The MWM test, as described previously (Chen et al., 2010), consisted of four days of training acquisition and an additional day of a probe trial with the water temperature kept at 23 ± 1°C. In the training trial, rats from 4 different quadrants were separately placed into a circle pool and allowed to find a platform hidden below 2 cm water within 120 s and then remain on the platform for 15 s; otherwise, the rats were manually guided to the platform. The intertrial interval for each rat was at least 5 min. In the probe trial, the platform was removed from the pool, and the number of times the rats crossed the platform site in 2 min was recorded (n = 5-6 per group; age = 65 weeks).

As previously described for the treadmill test (Martin-Montalvo et al., 2013), the rats were habituated at a constant speed of 5 m.min−1 for 5 min. The following day, each rat was given a trial starting at 7 m.min−1 for 5 min, 12 m.min−1 for 15 min, 15 m.min−1 for 45 min, and 19 m.min−1 for 135 min. The total distance run in the treadmill test was calculated until exhaustion, which was humanely defined as the time at which the animal's hind limbs made contact with the grid four times within a two-minute period (n = 5-6 per group; age = 66 weeks).

### Collection of blood and tissue

Animal blood was dynamically collected five times during the study using a tail-cut approach (n = 6-8 per group each time; survival experiment: age = 8, 28, 48, 68, 110 weeks; short-term experiment: age = 27 weeks). At the end of observation, the rats were anesthetized with chloral hydrate. The rats were deprived of food for 8 hours prior to blood collection, and serum was divided into several tubes for further measurement after being centrifuged at 3000 r/15 min at 4°C. Animal tissues were collected and weighed, and a portion of the tissue was fixed for pathology, while the remainder was rapidly frozen in liquid nitrogen and then stored at -80°C for further analysis. All procedures were carried out between 8 am and 12 pm.

### Indirect calorimetry

The indirect calorimetry (TSE, German) trial was conducted in a ventilated cabinet in a standard animal experimental environment (the details are as described above). Bedding material was used to cover the cage floor, and the rats were allowed to acclimate in respirometry cages for 2 hours prior to the start of measurement. The experiment began at 9 am and was monitored for 3 consecutive days. During this period, the rats had free access to water and were fed an isocaloric diet. Furthermore, stable air pressure and flow rates were considered important for acquiring meaningful calorimetry results. Food intake and body weight were recorded to confirm the health status of rats. Other measurements included O2 inhalation ($VO_2$) (i.e. O2 consumption) and $CO_2$ expiration ($VCO_2$) (i.e. $CO_2$ production) at 3-minute intervals. Respiratory exchange ratio (RER) and total energy expenditure (EE) (i.e. heat production) readouts were directly outputted to the computer. We collected the data from the last 2 days for analysis to avoid deviations caused by the new environment (n = 15, age = 68 weeks).

### Proteomics analysis

The livers of aging rats (age = 110 weeks) were collected, quickly frozen in liquid nitrogen, and prepared for proteomic analysis using iTRAQ-LC-MS/MS. The protocol was conducted as follows. i) Protein extraction and QC of protein extraction. Proteins were extracted with TissueLyser and further quantified by a Bradford assay. ii) Protein digestion. Trypsin digestion was performed with Trypsin Gold (Promega, Madison, WI, USA). iii) Peptide labeling. Peptide labeling was conducted with an ITRAQ Reagent 8-plex Kit according to the manufacturer's protocol. iv) Peptide fractionation. The peptides were separated using a Shimadzu LC-20AB

HPLC Pump system coupled with a high-pH RP column. v) HPLC for chromatographic separation. The separation was performed with an LC-20AD nano-HPLC instrument (Shimadzu, Kyoto, Japan) with a C18 trap column. vi) Mass spectrometer detection. The peptides separated from nano-HPLC were subjected to tandem mass spectrometry on a Q EXACTIVE (Thermo Fisher Scientific, San Jose, CA) for data-dependent acquisition (DDA) detection by nanoelectrospray ionization. vii) Data analysis. All proteins were identified with a 1% false discovery rate (FDR) and further enriched using DAVID (https://david.ncifcrf.gov/) for GO and KEGG analysis. PPI was performed in STRING (https://string-db.org/) and Cytoscape (version 3.6.1). A fold change of > 1.2 with a p value of < 0.05 was considered to be the cut off for differentially expressed proteins. Additional detailed protocols are as follows:

***Protein extraction***

(1) Mix 0.5 ml of lysis buffer 3 (8 M Urea, 40 mM Tris-HCl or TEAB with 1mM PMSF, 2mM EDTA and 10mM DTT, pH 8.5) with 100 mg of liver sample, and place in a 1.5 ml centrifuge tube.
(2) The mixtures were placed into a TissueLyser with two magnetic beads (diameter 5mm) for 2min at 50Hz to release proteins.
(3) Centrifugation with 25,000g at 4°C for 20min, and the supernatant was transferred into a new tube.
(4) Add 10 mM dithiothreitol (DTT) to the supernatant, and 56°C water bath for 1 hour.
(5) Return to room temperature and then alkylate by 55 mM iodoacetamide (IAM) in the dark at room temperature for 45min.
(6) Following centrifugation (25,000 g, 4°C, 20 min), the supernatant containing proteins was quantified by Bradford

***Quality control of protein extraction***

(1) Protein quantitation with bradford assay. Protein was quantitated according to the manufacturers' protocol.
(2) SDS-PAGE. After Mixing 30μg proteins with loading buffer in centrifuge tube, heat them at 95°C for 5 minutes to make protein sample. load the protein sample to holes in 12% polyacrylamide gel and then run SDS-PAGE at 120V constant voltage for 120 minutes. After electrophoresis, stain gel with Coomassie Blue for 2 hours, then add destaining solution (40% ethanol and 10% acetic acid) and shake it for 3-5 times, each time for 30 minutes.

***Protein digestion***

The protein solution (100ug) with 8M urea was diluted 4 times with 100mM TEAB. Protein was digested by Trypsin Gold (Promega, Madison, WI, USA) with the ratio of protein: trypsin = 40: 1 at 37°C overnight. After trypsin digestion, peptides were desalted with a Strata X C18 column (Phenomenex) and vacuum-dried according to the manufacturer's protocol.

***Peptide labeling***

The peptides were dissolved in 30ul 0.5M TEAB and vortex. Peptide labeling was conducted by ITRAQ Reagent 8-plex Kit (Sigma-Aldrich, Taufkirchen, Germany) according to the manufacturer's protocol. One unit of ITRAQ Reagent - 8-plex labels 60ug of protein digest. A total of eight samples were labeled with ITRAQ Reagent 8-plex Kit. The labeled peptides with different reagents were combined and desalted with a Strata X C18 column (Phenomenex) and vacuum-dried according to the manufacturer's protocol. The pH value was higher than 7.5 after labeling and the total labeling efficiency was 0.96%.

***Peptide fractionation***

The peptides were separated on a Shimadzu LC-20AB HPLC Pump system coupled with a high pH RP column. The peptides were reconstituted to 2 ml with mobile phase A (5% ACN, 95% $H_2O$, pH adjusted to 9.8 with ammonia) and loaded onto a column containing 5μm particles (phenomenex). Elute at a flow rate gradient of 1 ml/ min: 5% mobile phase B (5% $H_2O$, 95% ACN, adjust pH to 9.8 with ammonia) for 10 min, 5-35% mobile phase B for 40min, 35-95% mobile phase B for 1 min, 95% mobile phase B for 3 min and 5% mobile phase B for 10 min. Elution was monitored by measuring absorbance at 214 nm, and fractions were collected every 1 min. The eluted peptides were pooled as 20 fractions and vacuum-dried.

***HPLC***

Each fraction was resuspended in mobile phase A (2% ACN and 0.1% FA in water) and then centrifuged at 20,000 g for 10 min. The supernatant was loaded onto a C18 trap column 5 μl/min for 8min using a LC-20AD nano-HPLC instrument (Shimadzu, Kyoto, Japan) by the autosampler. Then, the peptides were eluted from trap column and separated by an analytical C18 column (inner diameter 75 μm) packed in-house. The gradient was as following at 300 nl/min: 5% mobile phase B (98% ACN, 0.1% FA) for 0-8 min; 8%-35% mobile phase B for 8-43 min; 35%-60% mobile phase B for 43-48 min; 60%-80% mobile phase B for 48-50 min; 80% mobile phase B for 50-55 min; 5% mobile phase B for 55-65 min.

***Mass spectrometer detection***

The peptides separated by nanoHPLC were ionized by nanoESI source and then subjected into the tandem mass spectrometry Q EXACTIVE (Thermo Fisher Scientific, San Jose, CA) for DDA (data-dependent acquisition) detection. The main parameters were listed as following: electrospray voltage: 1.6 kV; precursor scan range: 350-1600 m/z at a resolution of 70,000 in Orbitrap; MS/MS fragment scan range: >100 m/z at a resolution of 17,500 in HCD mode; normalized collision energy setting: 27%; dynamic exclusion time: 15 s; automatic gain control (AGC) for full MS target and MS2 target: 3e6 and1e5, respectively; the number of MS/MS scans following one MS scan: 20 most abundant precursorions above a threshold ion count of 20000. The instrument was operated in positive mode.

**Bioinformatics pipeline**

***MS/MS raw data***

Raw data must be converted to MGF files for bioinformatics analysis by thermo scientific tool Proteome Discoverer. For an MS/MS Ions Search, each query represents a complete MS/MS spectrum, and is delimited by a pair of statements: BEGIN IONS and END IONS.

### *MS/MS ion search and canonical proteomics database*

The exported MGF files were searched using Mascot version 2.3.02 in this project against the selected database. At least one unique peptide was necessary for the identified protein. Mascot search parameters are as follows:

| Item | Value |
|---|---|
| Type of search | MS/MS ion search |
| Enzyme | Trypsin |
| Fragment mass tolerance | 0.05Da |
| Mass values | Monoisotopic |
| Variable modifications | Oxidation (M), iTRAQ8plex (Y) |
| Peptide mass Tolerance | 20ppm |
| Fixed modifications | Carbamidomethyl (C), iTRAQ8plex (N-term), iTRAQ8plex (K) |
| Database | I-cxPBT002 (35814 sequences) |
| Database_info | Rtus_norvegicus(uniprot,20171117) |

### Protein quantification

An automated software called IQuant (Wen et al., 2014) was applied for quantitatively analyzing the labeled peptides with isobaric tags. To assess the confidence of peptides, the PSMs were pre-filtered at a PSM-level FDR of 1%. Then based on the "simple principle" (the parsimony principle), identified peptide sequences were assembled into a set of confident proteins. In order to control the false-positive rate of protein, the process filtered again at the protein level with 1% FDR (protein-level FDR < = 0.01) based on Picked protein FDR strategy. The protein quantification process included the following steps: protein identification, tag impurity correction, data normalization, missing value imputation, protein ratio calculation, statistical analysis and results presentation. IQuant quantitation parameters are as follows:

| Item | Value |
|---|---|
| Quant_peptide | Use All Unique peptide |
| Quant_number | At least one unique spetra |
| Normalization | VSN |
| Protein_Ratio | Weighted average |
| Statistical Analysis | Permutation Tests |

### *GO enrichment and pathway enrichment*

A total of 4830 proteins were identified and further enriched using DAVID (https://david.ncifcrf.gov/) for GO and KEGG analysis. PPI was performed in STRING (https://string-db.org/) and cytoscape (version 3.6.1). The fold changes of > 1.2 with p-values < 0.05 were considered as a cut off for differential proteins.

### Western blot analysis

Total protein from liver, kidney and muscle tissues from rats aged 28 or 110 weeks was extracted with RIPA lysis buffer (Beyotime, Shanghai, China) plus phenylmethanesulfonyl fluoride (PMSF) (Beyotime, Shanghai, China). The detailed western blot protocol used in our laboratory was described previously (Niu et al., 2013). The following antibodies were used for western blotting: FLOT1, CAT, GSK3β, FAS and ACC (Cell Signaling Technology, Beverly, MA, USA); CD36 and CPT1A (Abcam, Cambridge, MA, USA); PPARG (Cell Signaling Technology, Beverly, MA, USA or Wanleibio, Shenyang, China); NF-κB P65 and IL-6 (Wanleibio, Shenyang, China); NCALD (Absin, Shanghai, China); PPRC1 (Santa Cruz Biotechnology, CA, USA or OriGene Technologies, Origene, Maryland, USA); and β-actin, CPT2 and secondary antibody (Santa Cruz Biotechnology, Santa Cruz, CA, USA or Promega Biotech, Beijing, China).

### Quantitative real-time PCR

Total RNA was isolated from cells with TRIzol reagent (Invitrogen, CA, USA) according to the manufacturer's instructions. RNA was reverse transcribed to cDNA using a High-Capacity cDNA Reverse Transcription Kit (Applied Biosystems, CA, USA). Real-time PCR was performed with SYBR Green PCR Master Mix and the 7500 FAST Real-time PCR System (Applied Biosystems, CA,

USA). Human and rat β-actin gene primers were purchased from Sangon Biotech (Sangon Biotech, Jiangsu, China). The sequences of all primers are listed as follows:

| Primers | Sequences |
|---|---|
| fruit fly-rpl32-FORWARD | GCACTTCATCCGCCACCAGTC |
| fruit fly-rpl32-REVERSE | TGCGCTTGTTCGATCCGTAACC |
| fruit fly-dh-PPRC1(spargel)-FORWARD | AAGGAAGCACCAGCACCGAATG |
| fruit fly-dh-PPRC1(spargel)-REVERSE | GTGCCTCCAGCGTAGATGAACC |
| fruit fly-dh-PPARG(Eip75B)-FORWARD | CTCCACCATCAGCATCAGCATCAG |
| fruit fly-dh-PPARG(Eip75B)-REVERSE | CGCCGACTCCAGCAACTTGAC |
| fruit fly-whd-FORWARD | TGTTCGACCGCTGCTTGATGATG |
| fruit fly-whd-REVERSE | ACTCCTCCCACCAATCCGACAC |
| fruit fly-crq-FORWARD | TGCTGAACCATGAAGGCGGAAAG |
| fruit fly-crq-REVERSE | GCCACCCGAAGCGTTTGTAGG |
| fruit fly-cpt2-FORWARD | GCCGATGGGAAGGTGTTCATAGAC |
| fruit fly-cpt2-REVERSE | GCTACTGCTGCTCTGCTGGATG |
| fruit fly-acc-FORWARD | AGCAGGCAGGTCAGGTGTGG |
| fruit fly-acc-REVERSE | CAATCAGCGGCAACTCCTCTCG |
| fruit fly-dorsal-FORWARD | AGCAGCAGCAGCAGCAACAG |
| fruit fly-dorsal-REVERSE | TGCCGCCGAGAATTTACTTTCCC |
| fruit fly-cat-FORWARD | GAACGGCTATGGCTCGCACAC |
| fruit fly-cat-REVERSE | CCAACTGATCGGCGGTCTTCAC |
| human-actb- FORWARD | CCTGGCACCCAGCACAAT |
| human-actb- REVERSE | GGGCCGGACTCGTCATAC |
| human-pparg-FORWARD | AGATCATTTACACAATGCTGGC |
| human-pparg-REVERSE | TAAAGTCACCAAAAGGCTTTCG |
| human-pprc1-FORWARD | AACTACGGCTTCGTCACTTATC |
| human-pprc1-REVERSE | AGATCAGAATAGCTCCTCTTGC |
| rat-actb-FORWARD | TGTCACCAACTGGGACGATA |
| rat-actb- REVERSE | GGGGTGTTGAAGGTCTCAAA |
| rat-ncald-FORWARD | GCCAGATGGACACCAACAGAGATG |
| rat-ncald-REVERSE | GCAGGAGACGCACAATGGATGG |
| rat-flot1-FORWARD | TGGACATGCTGCTGGAGAAACTG |
| rat-flot1-REVERSE | CATGGTTCCGCTTCCGCTAGAC |
| rat-gsk3b-FORWARD | CAATCGCACTGTGTAGCCGTCTC |
| rat-gsk3b-REVERSE | GGTGTGTCTCGCCCATTTGGTAG |
| rat-pprc1-FORWARD | GCTGATGATCTGACACTGCCTGAG |
| rat-pprc1-REVERSE | GAATCTGCCGCACGACCACTG |
| rat-scot-FORWARD | GGGGTGTGCCTGCTACTTTTCC |
| rat-scot-REVERSE | ACACAACCCGAAACCACCAACC |

Data were normalized to endogenous ribosomal protein L32, human β-actin and rat β-actin gene expression in flies, humans and rats, respectively. All real-time primer sequences were validated for specificity and efficiency prior to use.

### Food intake measurement in Drosophila

The capillary feeder (CAFE) method described by Diegelmann et al. was used with some modifications (Diegelmann et al., 2017). Ten male flies aged 15 days were transferred to a fly chamber made of a fly vial maintained in an incubator at 25°C with 60% humidity. Ten chambers were set up as replicates. A 10 μL calibration capillary (VWR, West Chester, USA) was used to measure food intake on fly medium without agar by marking the food level, and mineral oil was added to each capillary to minimize food evaporation. After 24 h of feeding, food intake was recorded as the length (each 5 mm length is usually equal to 1 μL of liquid food) between the two markers on the feeding capillary minus the average length between the two markers on the evaporation control. Finally, Drosophila food intake was calculated by averaging the daily food consumption every three days.

## Quantification and statistical analysis

### Survival assessment

Animals were inspected daily, and rat trajectories were recorded in detail. Instant necropsy was carried out for dead and euthanized animals, and animal tissues and blood were collected for further diagnosis of causes of death. The criteria for euthanasia were estimated by a veterinarian according to AAALAC guidelines, and only cases where the condition of the animals was considered inharmonious with continued survival were recorded as deaths. The experiment did not end until at least half of the animals from each group died. Finally, survival curves were plotted using the Kaplan-Meier method.

### Pathology examinations and quantification

Tissues (tumor, brain, heart, liver, kidney, lung, and spleen) were fixed in 4% paraformaldehyde and embedded in paraffin, and 6-μm-thick sections were stained with hematoxylin and eosin (H&E). Histological examinations were performed by pathologists blinded to the groups. Additionally, the liver, kidney and lung were further scored for age-associated pathological changes, as previously described (Niu et al., 2013; Xie et al., 2017). At least 3-8 fields were scored.

### Blood chemistry measurement

A broad range of serum parameters, including GLU, TCHO, TG, LDL-C, HDL-C, AST, ALT BUN and CRE, were dynamically quantified using a ROCHE Modular P800 Automatic Biochemical Analyzer (Roche Diagnostics, Mannheim, Germany) at different time points (survival experiment: age = 8, 28, 48, 68, and 110 weeks; short-term experiment: age = 27 weeks). SOD, GSH, MDA and NO were dynamically determined with commercial kits employing enzymatic methods (Beyotime, Shanghai, China) at 28, 68, and 110 weeks. ROS, TNF-α, IL-6 (Biotopped, Beijing, China) and insulin (Westang, Shanghai, China) were assayed using ELISA kits at 28, 68, and 110 weeks, according to the manufacturers' protocol (n = 6-8 per group at each time).

### Free fatty acids measurement

The levels of FFAs in rat serum, liver, kidney and muscle (n = 7-10, age = 28 and 68 weeks), as well as in Drosophila (200 mg, age = 15 days), were measured by GC/MS-MS analysis using a TRACE 1310 gas chromatograph equipped with a Helium TSQ 8000 Evo mass spectrometer (Thermo Finnigan, Austin, TX, USA), as described in our earlier study with some modifications (Liu et al., 2018).

### Blood beta-hydroxybutyrate levels

Blood beta-hydroxybutyrate (BHB) levels in rats were measured using kits (Jining, Shanghai, China), according to the manufacturer's instructions. (n = 6-8, age = 28, 68, and 110 weeks)

### Statistical analysis

Unless otherwise stated, data are presented as the mean ± SEM. Student's t test or one-way ANOVA with various post hoc tests, nonparametric tests or survival analysis was used for all comparisons, and two-way ANOVA was used to analyze the between-subjects factors of time and diet. A p value $< 0.05$ was considered statistically significant. Statistical calculations were carried out with GraphPad Software (version 7), SPSS 17.0 (SPSS, Chicago, IL, USA) or R (version 3.5.1).

**Cell Metabolism, Volume *33***

## Supplemental information

# An isocaloric moderately high-fat diet extends lifespan in male rats and *Drosophila*

**Dan Shi, TianShu Han, Xia Chu, Huimin Lu, Xue Yang, TianQi Zi, YanHe Zhao, XinYue Wang, ZhiPeng Liu, JingQi Ruan, Xin Liu, Hua Ning, MaoQing Wang, Zhen Tian, Wei Wei, Yue Sun, YinLing Li, Rui Guo, Yu Wang, Fan Ling, Yue Guan, Da Shen, YuCun Niu, Ying Li, and ChangHao Sun**

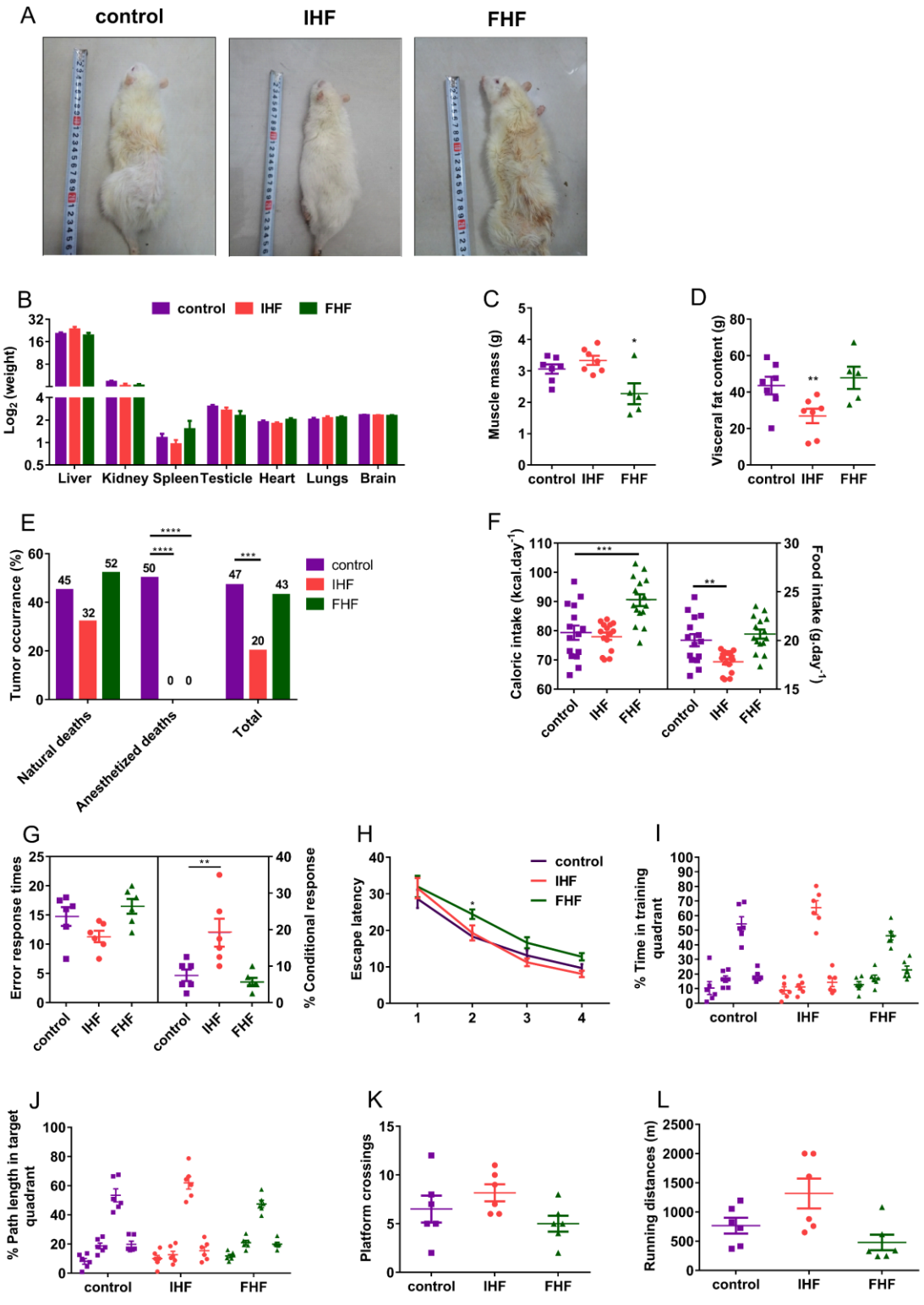


**Figure S1. Representative images, body composition and healthspan tests of activity and physical function in rats. Related to Figure 1.**

**(A)** Representative images depicting animal.

**(B)** Organ weights. Organ mass values are expressed as the log2 value relative to total body weight (control: n = 7 rats, IHF: n = 10 rats, FHF: n = 5 rats, 110 weeks, male).

**(C)** Muscle mass (control: n = 7 rats, IHF: n = 7 rats, FHF: n = 5 rats, 110 weeks, male).

**(D)** Visceral content (control: n = 7 rats, IHF: n = 7 rats, FHF: n = 5 rats, 110 weeks, male).

**(E)** Tumor occurrence in naturally deceased animals and those culled at 110 weeks of age (natural deaths, control: n = 22 rats, IHF: n = 19 rats, FHF: n = 25 rats; anesthetized deaths, control: n = 8 rats, IHF: n = 11 rats, FHF: n = 5 rats). Statistical analyses were performed using Chi-square test or Fisher exact test.

**(F)** Left: caloric intake in metabolic cages. Right: food intake in metabolic cages (n = 15 rats per group, 68 weeks, male).

**(G)** Shuttle box test. Left: error response times. Right: proportion of conditional response.

**(H-K)** Morris water maze test. **(H)** Escape latency, **(I)** proportion of time in training quadrant, **(J)** proportion of path length in target quadrant and **(K)** platform crossings.

**(L)** Treadmill test. Running distances.

Error bars, when present, show the SEM. (control: n = 6 rats, IHF: n = 6 rats, FHF: n = 6 rats, 66 weeks, male). *p < 0.05, **p < 0.01, ***p < 0.001, ****p < 0.0001 versus control.

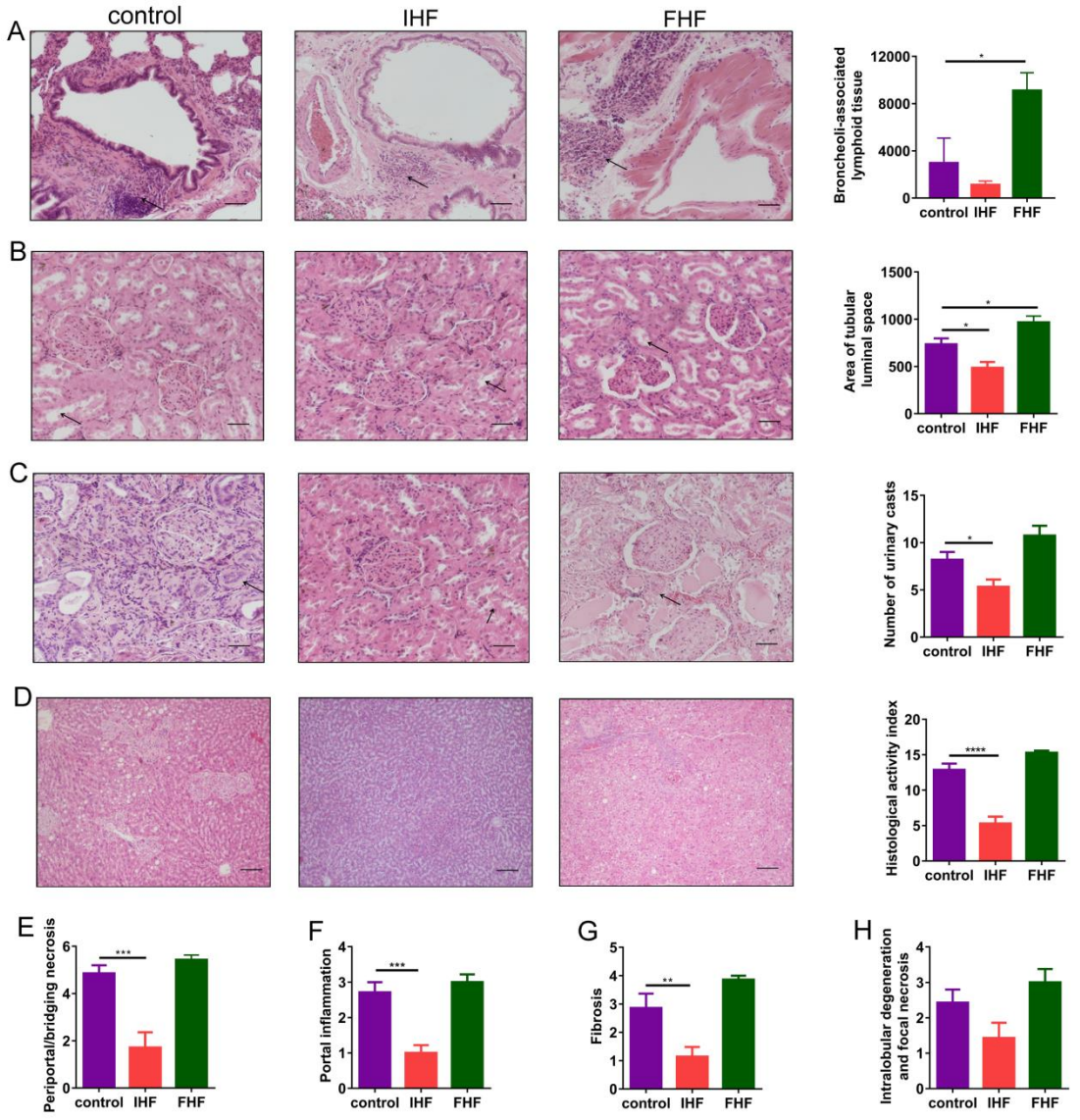


**Figure S2. IHF effects on aging-related pathology in the lung, kidney and liver. Related to Figure 1.**

**(A-H)** Histopathology. Representative images of sections derived from the **(A)** lung (scale bar = 20 μm), **(B-C)** kidney (scale bar = 20 μm) and **(D)** liver (scale bar = 20 μm) are shown on the left. Quantification of **(A)** broncheoli-associated lymphoid tissue (indicated by arrows), **(B)** area of tubular luminal space (indicated by arrows), **(C)** numbers of urinary casts (indicated by arrows) and **(D)** histological activity index (HAI) is presented in the panels on the right. Quantification of **(E)** periportal/bridging necrosis, **(F)** portal inflammation, **(G)** fibrosis, **(H)** intralobular degeneration and focal necrosis.

Error bars, when present, show the SEM. (control: n = 6-7 rats, IHF: n = 6-8 rats, FHF = 5 rats, 110 weeks, male). *p < 0.05 between diets, **p < 0.01 between diets, ***p < 0.001 between diets, ****p < 0.0001 between diets.

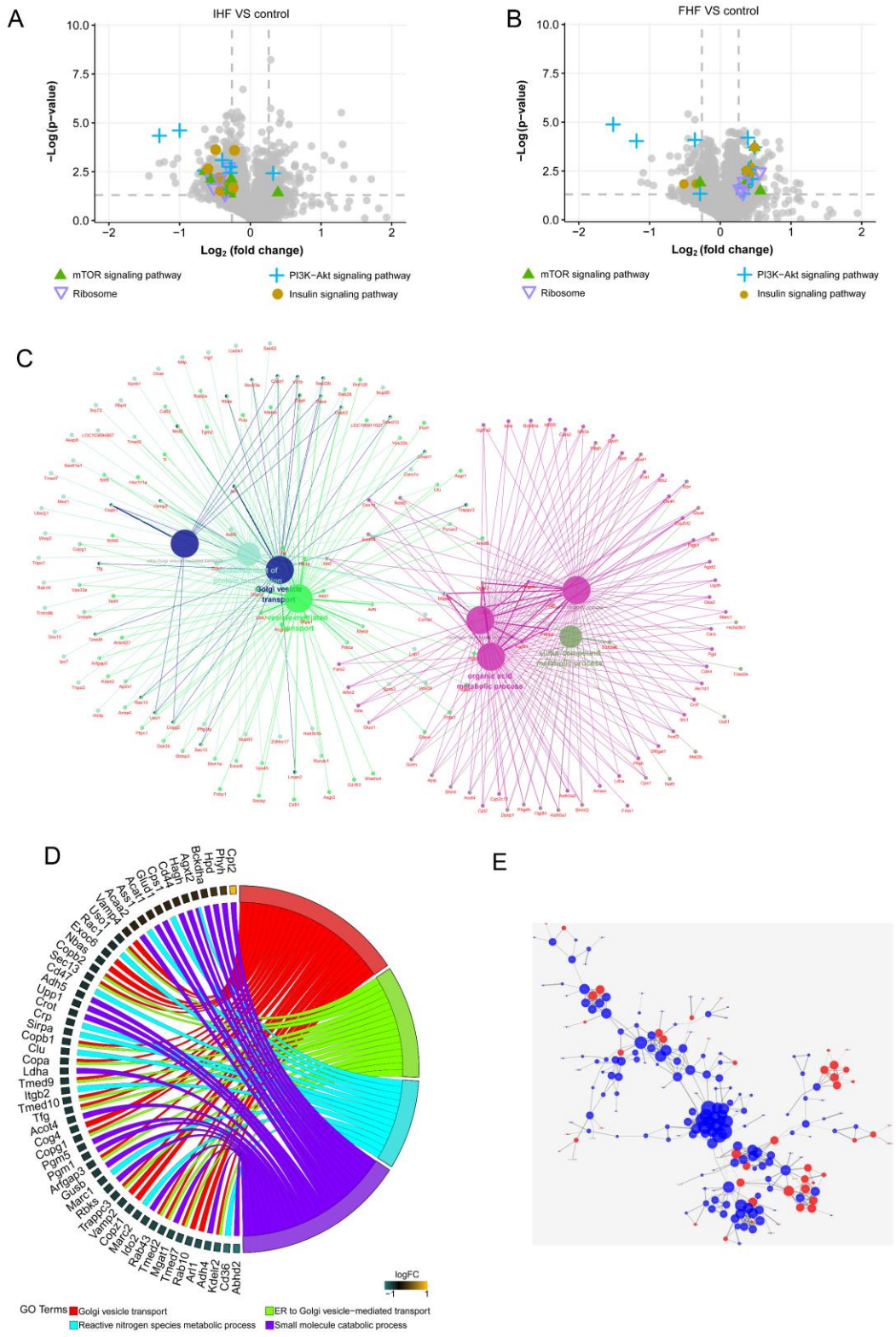


**Figure S3. KEGG analysis, GO analysis, clusterProfiler analysis and protein-protein interactions. Related to Figure 4.**

**(A)** KEGG related proteins to pathways with regard to mTOR signaling

pathway, PI3K-Akt signaling pathway, ribosome and insulin signaling pathway in response to the IHF diet.

**(B)** KEGG related proteins to pathways with regard to mTOR signaling pathway, PI3K-Akt signaling pathway, ribosome and insulin signaling pathway upon in response to the FHF diet.

**(C)** GO analysis. All differentially expressed proteins in response to the IHF diet were analyzed and plotted using Cytoscape ClueGO (only pathways with $p \leqq 0.001$ are shown).

**(D)** ClusterProfiler analysis of all differentially expressed proteins upon IHF, showing items that were remarkably significantly related to Golgi vesicle transport, ER to Golgi vesicle-mediated transport, reactive nitrogen species metabolic process and small molecule catabolic process.

**(E)** Protein-protein interaction analysis. All differentially expressed proteins in response to the IHF diet were plotted using STRING and Cytoscape.

Error bars, when present, show the SEM. Also see Data S1 and S2.

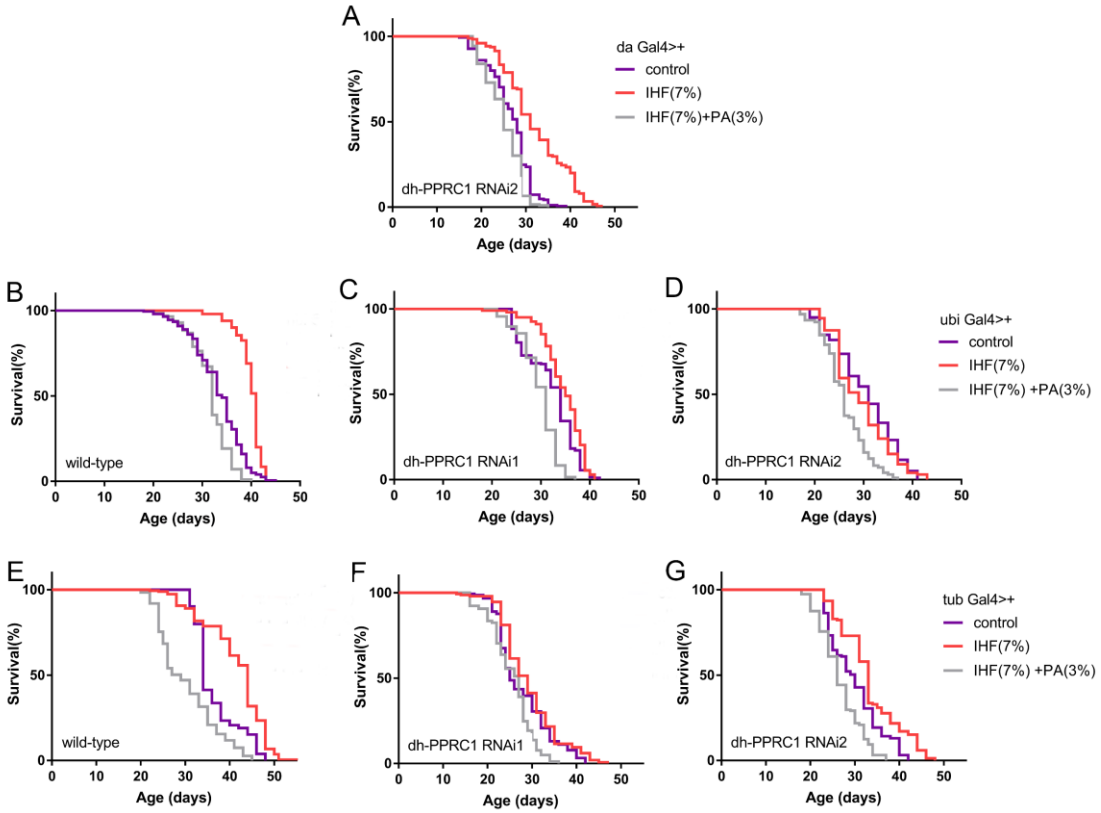


**Figure S4. Reduction of lifespan extension upon IHF in flies with mutations in dh-PPRC1 genes. Related to Figure 6.**

**(A)** IHF extended lifespan in dh-PPRC1 RNAi2 mutants driven by daGal4 ($p < 0.0001$, log-rank test; n = 165-199 flies per group), but lifespan extension upon IHF in wild-type flies (20.6%) was larger than that in dh-PPRC1 RNAi2 mutants (10.7%) ($p < 0.0001$, two-way ANOVA). PA impaired IHF-mediated lifespan extension in dh-PPRC1 RNAi2 mutants driven by daGal4 ($p < 0.0001$, log-rank test; n = 175-199 flies per group), but lifespan impairment driven by PA upon IHF in wild-type flies (31.7%) was larger than that in dh-PPRC1 RNAi2 mutants (19.4%) ($p < 0.0001$, two-way ANOVA). Also see Table S9 for lifespan statistics.

**(B-D)** IHF extended lifespan in both wild-type flies and dh-PPRC1 RNAi1 mutants driven by ubiGal4, but not in dh-PPRC1 RNAi2 mutants ($p < 0.0001$, $p = 0.0001$ and $p = 0.1392$ respectively, log-rank test; n = 195-203 flies per group), and lifespan extension upon IHF in **(B)** wild-type flies (20.6%) was larger than that in **(C)** dh-PPRC1 RNAi1 mutants (2.9%) or **(D)** dh-PPRC1

RNAi2 (6.5%) ($p < 0.0001$, two-way ANOVA). PA impaired IHF-mediated lifespan extension in both wild-type flies and dh-PPRC1 RNAi1 mutants driven by ubiGal4, as well as in dh-PPRC1 RNAi2 mutants ($p < 0.0001$ for all comparison, log-rank test; n = 195-203 flies per group), but lifespan impairment driven by PA upon IHF in **(B)** wild-type flies (22%) was larger than that in **(C)** dh-PPRC1 RNAi1 mutants (11.4%) or **(D)** dh-PPRC1 RNAi2 (10.3%) ($p < 0.0001$, two-way ANOVA). Also see Table S9 for lifespan statistics.

**(E-G)** IHF extended lifespan in wild-type flies, dh-PPRC1 RNAi1 mutants or dh-PPRC1 RNAi2 mutants driven by tubGal4 ($p < 0.0001$, $p = 0.0106$ and $p < 0.0001$ respectively, log-rank test; n = 148-192 flies per group), but lifespan extension upon IHF in **(E)** wild-type flies (29.4%) was larger than that in **(F)** dh-PPRC1 RNAi1 mutants (16%) or **(G)** dh-PPRC1 RNAi2 (10%) ($p < 0.0001$, two-way ANOVA). PA impaired IHF-mediated lifespan extension in wild-type flies, dh-PPRC1 RNAi1 mutants and dh-PPRC1 RNAi2 mutants driven by tubGal4 ($p < 0.0001$ for all comparison, log-rank test; n = 148-192 flies per group), but lifespan impairment driven by PA upon IHF in **(E)** wild-type flies (34.1%) was larger than that in **(F)** dh-PPRC1 RNAi1 mutants (6.9%) or **(G)** dh-PPRC1 RNAi2 (21.2%) ($P < 0.0001$, two-way ANOVA). Also see Data S3 for lifespan statistics.

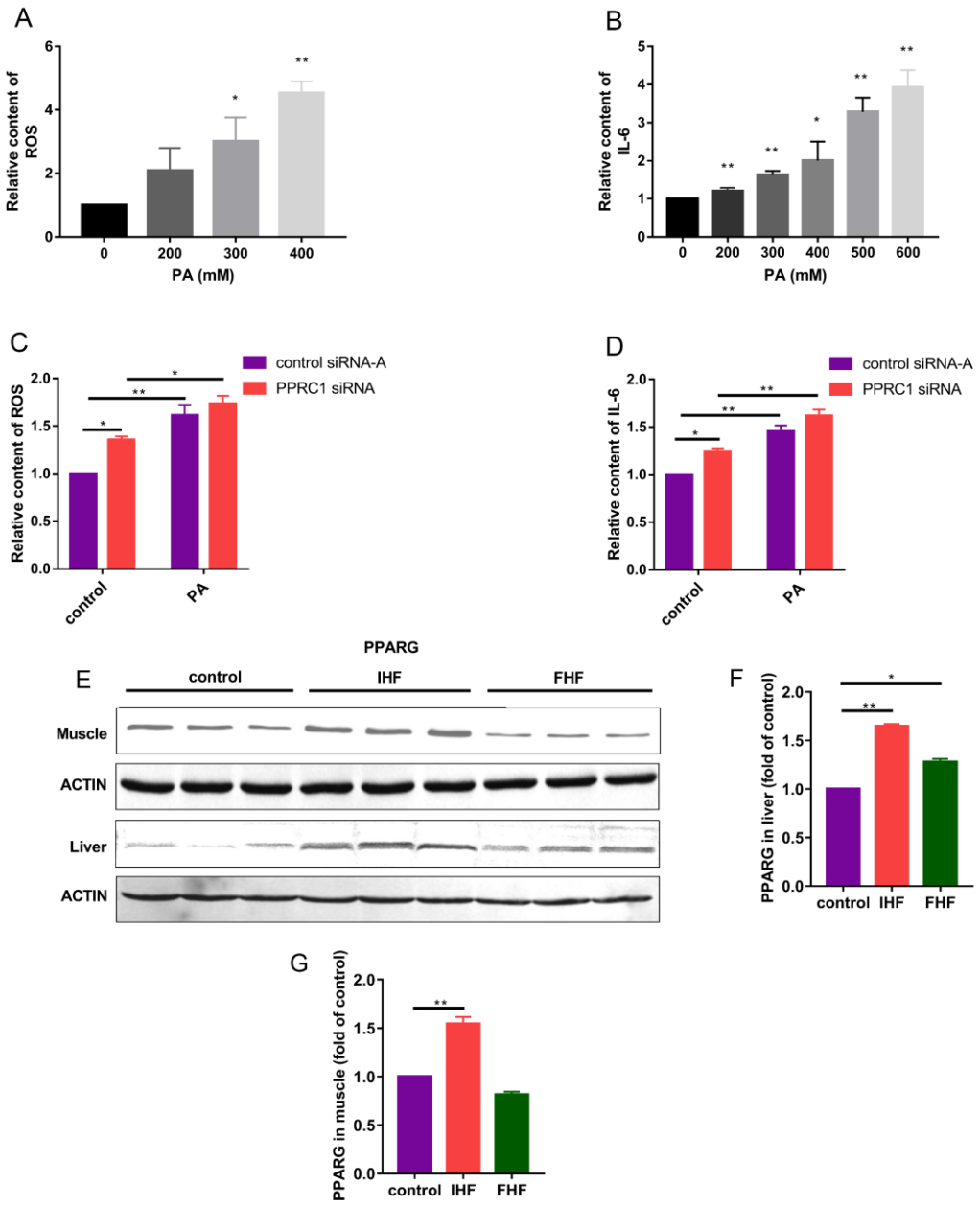


**Figure S5. ROS and IL-6 level in HepG2 cells and PPARG expression levels in rats. Related to Figure 7.**

**(A-B)** Different levels of PA affected **(A)** ROS and **(B)** IL-6 level in HepG2 cells (n = 3-5). *Compared with PA 0 mM, ** $p < 0.05$, ** $p < 0.01$.

**(C-D)** PA affected **(C)** ROS and **(D)** IL-6 levels in HepG2 cells treated with PPRC1 siRNA (n = 3-4).

**(E-G)** Protein expression was detected by western blot in the muscle and liver of rats. **(E)** Representative blots are shown for each protein. A representative

loading control is shown for each case (n=3). **(F-G)** Quantification of PPARG protein levels in the **(F)** liver and **(G)** muscle tissue.

Error bars, when present, show the SEM. *p < 0.05 between diets, **p < 0.01 between diets, ***p < 0.001 between diets, ****p < 0.0001 between diets.

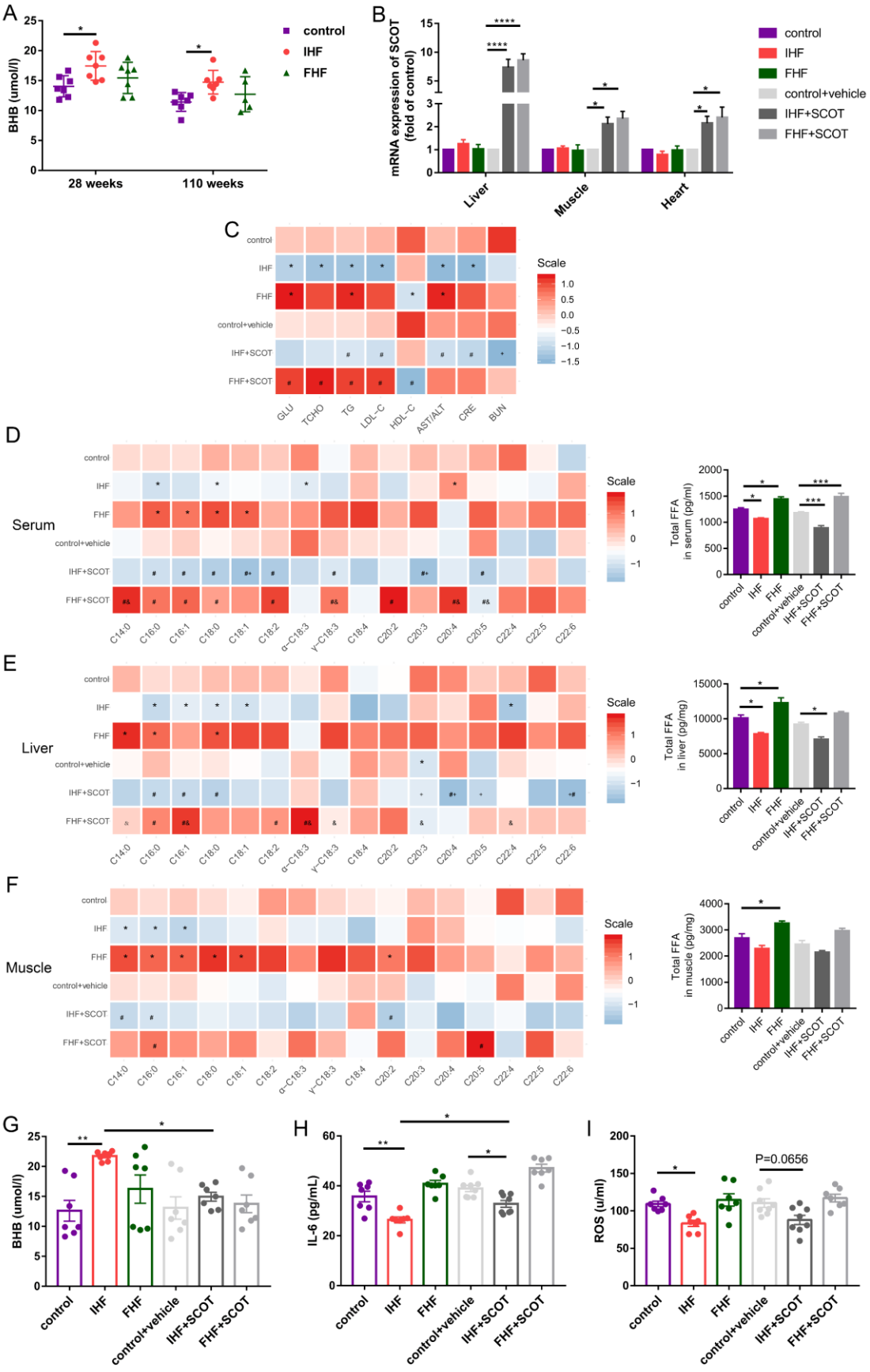
A
BHB (umol/l)
28 weeks
110 weeks
control
IHF
FHF
B
mRNA expression of SCOT (fold of control)
Liver
Muscle
Heart
control
IHF
FHF
control+vehicle
IHF+SCOT
FHF+SCOT
C
Scale
GLU
TCHO
TG
LDL-C
HDL-C
AST/ALT
CRE
BUN
D
Serum
Total FFA in serum (pg/ml)
E
Liver
Total FFA in liver (pg/mg)
F
Muscle
Total FFA in muscle (pg/mg)
C14:0
C16:0
C16:1
C18:0
C18:1
C18:2
α−C18:3
γ−C18:3
C18:4
C20:2
C20:3
C20:4
C20:5
C22:4
C22:5
C22:6
G
BHB (umol/l)
H
IL-6 (pg/mL)
I
ROS (u/ml)
P=0.0656

**Figure S6. BHB is a secondary factor responsible for reduction of oxidative stress and inflammation upon IHF. Related to the STAR Methods of Animals and diets.**

**(A)** Serum beta-hydroxybutyrate (BHB) levels were measured in male rats during the survival experiment (n=7 rats per group, 28 weeks male; control: n = 7 rats, IHF: n =7 rats, IHF: n = 5 rats, 110 weeks, male).

**(B-I)** Short-term animal intervention experiment. **(B)** Scot mRNA expression in liver, muscle and heart. **(C)** Serum measures related to glucose, lipids, and liver and kidney function. **(D-F)** Left: free fatty acids (FFAs) profiles and right: total FFA concentrations in the **(D)** serum, **(E)** liver and **(F)** muscle. *Compared with control, *$p < 0.05$; $^{\#}$Compared with control+vehicle, $^{\#}p < 0.05$; $^{+}$Compared with IHF, $^{+}p < 0.05$; $^{\&}$Compared with FHF, $^{\&}p < 0.05$. **(G)** Serum beta -hydroxybutyrate (BHB) levels were measured in male rats. **(H)** Serum IL-6 levels were measured in male rats. **(I)** Serum ROS levels were measured in male rats (n = 7-8 rats per group, 25 weeks, male).

Error bars, when present, show the SEM. *$p < 0.05$ between diets, **$p < 0.01$ between diets, ***$p < 0.001$ between diets, ****$p < 0.0001$ between diets.

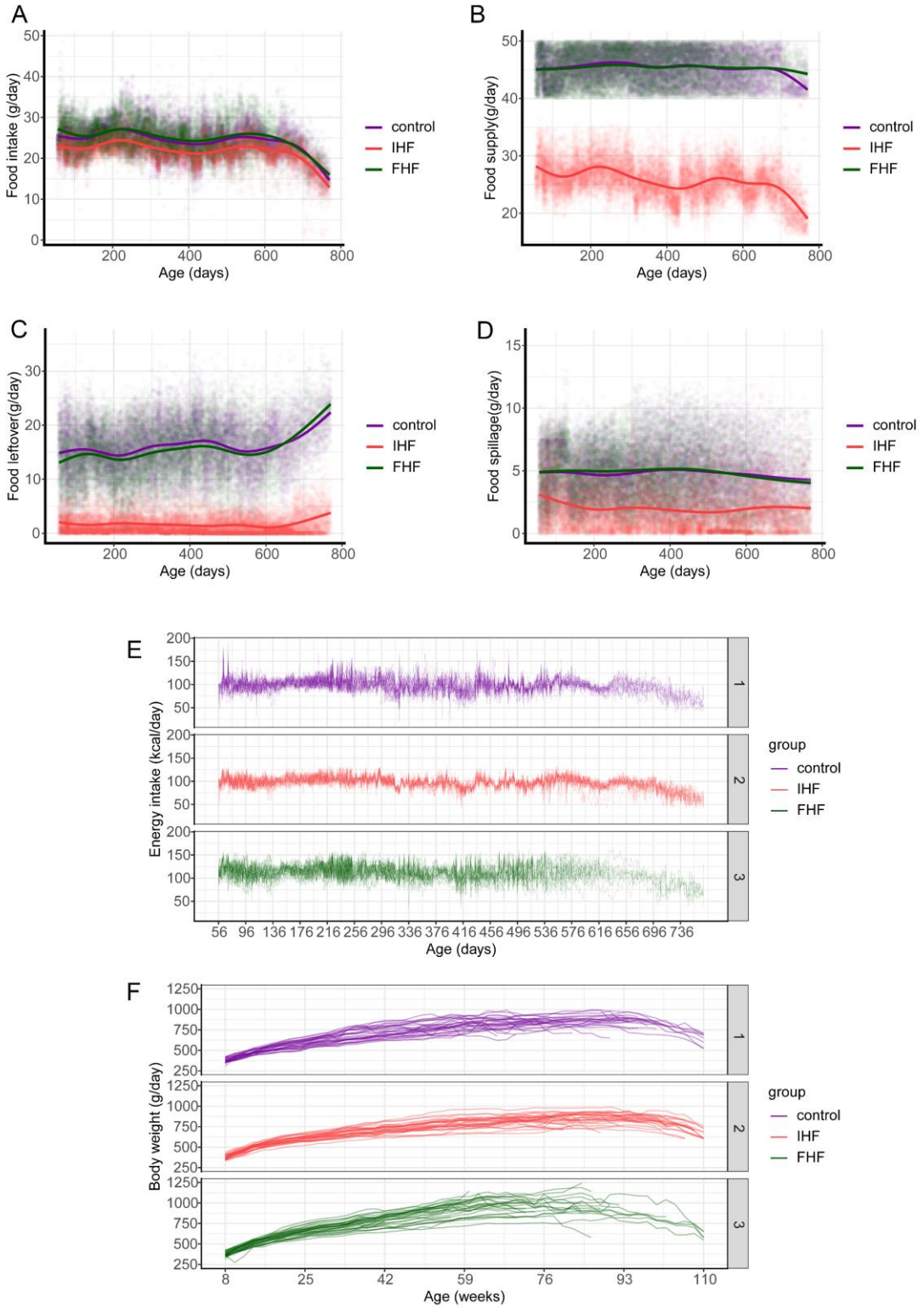


**Figure S7. Daily energy intake, daily food intake and biweekly body weight for each single-housed rat. Related to the STAR Methods of Animals and diets.**

**(A)** Daily food intake trajectories for each single-housed rat (n = 30 rats per

group in the beginning).

**(B)** Daily food supply trajectories for each single-housed rat (n = 30 rats per group in the beginning).

**(C)** Daily food leftover trajectories for each single-housed rat (n = 30 rats per group in the beginning).

**(D)** Daily food spillage trajectories for each single-housed rat (n = 30 rats per group in the beginning).

**(E)** Daily Energy intake trajectories for each single-housed rat (n = 30 rats per group in the beginning).

**(F)** Biweekly Body weight trajectories for each single-housed rat (n = 30 rats per group in the beginning).

Every dot referred to each record for daily food intake **(A)**, daily food supply **(B)**, daily food leftover **(C)** and daily food spillage **(D)**. Every line referred to each single-housed rat for daily energy intake **(E)** and body weight (F).

**Table S1. Necropsy data, cause of natural deaths determined by a veterinary pathologist in male rats. Related to Figure 1 and Figure S1.**

| Organ | Pathology | Control (n=22) | IHF (n=19) | FHF (n=25) |
|---|---|---|---|---|
| Head | Focal subarachnoid hemorrhage | 1 | 0 | 0 |
| | Pituitary adenoma | 1 | 2 | 2 |
| | Hepatocellular carcinoma | 1 | 0 | 0 |
| | Unspecified tumor | 1 | 2 | 0 |
| Lung | Congestion, mononuclear cells infiltration | 4 | 1 | 1 |
| | Squamous cell carcinoma | 0 | 0 | 1 |
| Liver | Inflammatory cell infiltration, punctate necrosis, fatty steatosis | 12 | 6 | 18 |
| | Hepatocellular carcinoma | 0 | 0 | 1 |
| Kidney | Fibrosis, transparent degeneration, hyperplasia | 10 | 3 | 10 |
| Spleen | Hemorrhage | 4 | 3 | 2 |
| Body cavity | Mucoid carcinoma | 0 | 0 | 1 |
| | Lymphoma | 2 | 0 | 1 |
| | Adenocarcinoma | 0 | 0 | 1 |
| | Unspecified tumor | 0 | 1 | 0 |
| Subcutaneous | Fibroma | 1 | 0 | 0 |
| | Squamous cell carcinoma | 3 | 1 | 3 |
| | Subcutaneous fibrosarcoma | 1 | 0 | 1 |
| | Myxoma (unspecified tumor) | 1 | 0 | 2 |
| Others | Pleural/Peritoneal effusion | 4 | 0 | 2 |

Note: multiple pathology changes were showed in each rat.

**Table S2. Pathological tumor classification determined by a veterinary pathologist in male rats. Related to Figure 1 and Figure S1.**

| Location | Tumor | Natural deaths | | | Anesthetized deaths | | |
|---|---|---|---|---|---|---|---|
| | | Control (n=22) | IHF (n=19) | FHF (n=25) | Control (n=8) | IHF (n=11) | FHF (n=5) |
| Head | Hepatocellular carcinoma | 1 | 0 | 0 | 0 | 0 | 0 |
| | Pituitary adenoma | 1 | 2 | 2 | 2 | 0 | 0 |
| | Unspecified tumor | 1 | 2 | 0 | 0 | 0 | 0 |
| Thoracic cavities | Lymphoma | 2 | 0 | 0 | 0 | 0 | 0 |
| | Squamous cell carcinoma | 0 | 0 | 1 | 0 | 0 | 0 |
| | Myxoma (unspecified tumor) | 0 | 1 | 0 | 0 | 0 | 0 |
| Abdominal cavities | Hepatocellular carcinoma | 0 | 0 | 1 | 2 | 0 | 0 |
| | Adenocarcinoma | 0 | 0 | 1 | 0 | 0 | 0 |
| | Lymphoma | 0 | 0 | 1 | 0 | 0 | 0 |
| | Mucoid carcinoma | 0 | 0 | 1 | 0 | 0 | 0 |
| | Epitheliogenic tumor (unspecified tumor) | 0 | 0 | 0 | 1 | 0 | 0 |
| Subcutaneous | Squamous cell carcinoma | 3 | 1 | 3 | 0 | 0 | 0 |
| | Subcutaneous fibrosarcoma | 1 | 0 | 1 | 0 | 0 | 0 |
| | Fibroma | 1 | 0 | 0 | 0 | 0 | 0 |
| | Myxoma (unspecified tumor) | 1 | 0 | 2 | 0 | 0 | 0 |

**Table S3. Recipes used for larval media and fly media for survival analyses (w/v). Related to the STAR Methods of Drosophila stocks.**

| Component (g) | Larval media | Control (0%) | IHF (3%) | IHF (7%) | IHF (10%) |
|---|---|---|---|---|---|
| Agar | 10 | 11 | 11 | 11 | 11 |
| Dextrose | 55 | 145 | 103.53 | 48.29 | 1.52 |
| Corn meal | 60 | 50 | 50 | 50 | 50 |
| Sucrose | 30 | 91 | 64.97 | 30.3 | 9.56 |
| Yeast | 25 | 18 | 18 | 18 | 18 |
| 20% Tegosept | 15 | 15 | 15 | 15 | 15 |
| Propionic acid | 3 | 3 | 3 | 3 | 3 |
| Lard | 0 | 0 | 30 | 70 | 100 |
| Water | 1000ml | 1000ml | 1000ml | 1000ml | 1000ml |
| Calorie (cal) | | | | | |
| Carbohydrate | — | 1087.45 | 817.45 | 457.81 | 187.77 |
| Protein | — | 75.46 | 75.46 | 75.46 | 75.46 |
| Fat | — | 15.50 | 285.50 | 645.50 | 915.50 |
| Total calorie | — | 1178.402 | 1178.402 | 1178.762 | 1178.722 |

3% (w/v) PA media: The media recipe is applied to assay the response of flies to various concentrations of PA. The media type is same as 0% or 7% (w/v) fly media differing only in the amount of PA used.

7% (w/v) FHF media: The media type is adding 7% (w/v) lard on the basis of 0% (w/v) control lard media.

**Table S4. Average food composition intakes per day. Related to the STAR Methods of Animals and diets.**

| Component (g/day) | Control | IHF | FHF | p1 | p2 |
|---|---|---|---|---|---|
| Casein | 4.972±0.328 | 4.877±0.283 | 5.09±0.321 | 0.393 | 0.2488 |
| L-cystine | 0.075±0.005 | 0.077±0.004 | 0.076±0.005 | 0.2087 | 0.6215 |
| Cornstarch | 9.882±0.651 | 6.739±0.391 | 8.284±0.522 | 0.0001 | 0.0001 |
| Dextrinized cornstarch | 3.282±0.216 | 2.532±0.147 | 2.901±0.183 | 0.0001 | 0.0001 |
| Sucrose | 2.486±0.164 | 1.77±0.103 | 2.24±0.141 | 0.0001 | 0.0001 |
| Soybean oil | 1.74±0.115 | 1.549±0.09 | 1.782±0.112 | 0.0001 | 0.223 |
| Lard | 0±0 | 2.213±0.128 | 2.596±0.164 | 0.0001 | 0.0001 |
| Mixed minerals | 0.87±0.057 | 0.854±0.05 | 0.891±0.056 | 0.4184 | 0.2377 |
| Mixed vitamins | 0.249±0.016 | 0.243±0.128 | 0.255±0.016 | 0.9325 | 0.9325 |
| Cellulose | 1.243±0.082 | 1.219±0.071 | 1.273±0.08 | 0.3858 | 0.2382 |
| Choline | 0.062±0.004 | 0.055±0.003 | 0.064±0.004 | 0.0001 | 0.0713 |

Note: All values are mean ± SD. (n = 30 per group). p1: IHF and control were compared using one-way ANOVA. p2: FHF and control were compared using one-way ANOVA.